ENVISIONING THE WORLD OCEAN

PARTIAL PRELIMINARY VERSION

Peter K. Weyl

December 20 1993

ENVISIONING - To Picture in the Mind

MARINE SCIENCES RESEARCH CENTER

STATE UNIVERSITY OF NEW YORK

ENVISIONING THE WORLD OCEAN

PARTIAL PRELIMINARY VERSION

Peter K. Weyl

December 20 1993

ENVISIONING - To Picture in the Mind

Stony Brook New York

Special Report 107

Reference No. 93-7

Approved for Distribution

J.R.Schubel

J.R.Schubel
Dean and Director

© Peter K. Weyl 1993

TABLE OF CONTENTS

File:/ENV_1\ENV_FRNT

PREFACE

Paraphrasing Dickens: These are the best and the worst of times to attempt to envision the World Ocean.

These are the best of times because recent and continuing developments in micro computer hardware and software have revolutionized our ability to access quantitative information about the World Ocean and display it in a variety of graphic formats which facilitate envisioning its behavior.

These are the worst of times because the technology for envisioning is still in a state of rapid evolution and because the needs of the generalist are overwhelmed by the flood of scientific publications. Because of the former, there is little point to document the current methodology for envisioning. Because of the latter, it becomes ever more difficult to keep informed of significant advances in observation and theory that can contribute to a better understanding of the behavior of the World Ocean.

To place this partial preliminary version of **Envisioning the World Ocean** in perspective, I start with a brief synopsis of my past scientific endeavors:

My scientific career began in low energy experimental nuclear physics. After finishing a doctoral thesis measuring the energy loss of ions in gases at the University of Chicago under Professor Samuel K. Allison, I spent a year at the Brazilian Center for Physical Research in Rio de Janeiro trying to set up a laboratory.

Returning to the United States, I was hired by the Exploration and Production Research Laboratory of Shell Oil Company in Houston, Texas to study the thermoluminescence of sedimentary rocks. The more I learned about this complex phenomenon, the less hope I saw for its practical application to the oil business. I developed a second order theory of the phenomenon and, with colleagues, by irradiating and deforming limestone, we miraculously managed to change its color to blue. As far as I know, the main applications of thermoluminescense, since then, have been as a radiation dosimeter and to distinguish ancient pottery from modern fakes.

Learning about the need to find sedimentary rocks with porosity and permeability that could hold petroleum and permit it to flow, I started to investigate the transformation of sediments into sedimentary rock. My initial efforts resulted in a theory of pressure solution and explained the formation of stylolites.

I started thinking about sandstones but, fortunately, interaction with the carbonate geologists at Shell soon drew my attention to carbonate rocks and the chemistry of sea water. Having vacationed as a child in the Dolomite mountains of Italy, I became fascinated by the dolomite problem. Marine organisms deposit skeletal material of calcium carbonate derived from seawater. The best carbonate rocks for petroleum reservoirs,however, consist of the magnesium - calcium carbonate mineral dolomite. There is more magnesium than calcium in sea water, but no marine organism has ever been found that uses this mineral to build its architecture.

In pursuit of the dolomite problem, Ken Deffeyes and I first immersed ourselves in San Francisco Bay to study the chemistry of its salt ponds, using a ladder and two inner tubes as our research vessel. To better determine the solubility of carbonates in sea water, I invented the carbonate saturometer, a simple device that determines dissolution or precipitation by the change in pH of the water when a carbonate mineral is introduced. I first used this instrument in 1960 on a cruise in the Gulf of Mexico as guest of Donald Hood on the research vessel Hidalgo of Texas A & M.

The saturometer works fine in essentially fresh water; however, its results in seawater proved puzzling. Countless experiments in the laboratory and at sea demonstrated that seawater does not come to equilibrium with carbonate minerals. Rather, the surface layers of the minerals equilibrate with the sea and each other. Any handful of carbonate sediments documents the long term coexistence of many phases in sea water in apparent violation of the Gibbs phase rule. In spite of, or perhaps because it can not be determined, the futile quest for the "true" solubility of carbonate phases in sea water continues.

A 1961 trip with Deffeyes and Lucia to the Caribbean Island of Bonaire provided the answers to the Dolomite problem. In the south, this island had evaporite ponds where the magnesium to calcium ratio was increased by calcium carbonate and gypsum deposition as the result of biological precipitation and evaporation. The dense brines then reflux to the ocean through the island's sediments, returning dense brines with a greatly increased magnesium/calcium ratio to the sea. In the northern, elevated parts of the island we could show how reflux of such brines during the Plio-Pleistocene, from evaporite ponds that have since eroded, had converted biogenic marine limestones to dolomite.

Our model for dolomite formation was challenged by stable isotope "experts" who contended that their isotopic salinity scale precluded an evaporite origin for dolomite. The theoretical model on which the isotopic salinity scale was based assumed evaporation of seawater into a perfect vacuum. A more realistic

model of seawater evaporation into heated quasi-saturated air from coastal evaporite lagoons supported by field observations on the island of Inagua invalidated the simplistic isotopic paleo-salinity scale.

About this time my colleague, King Hubbert, showed that the future chance of finding significant new petroleum reserves in the United States were slim. I was one of the few who took his projections seriously and decided that there was little future for basic research to improve the art of petroleum exploration.

I therefore terminated my career as a nuclear physicist in the chemistry department of an oil company working on geological problems and went to the Department of Oceanography at Oregon State University as Professor of Chemical Oceanography. While learning oceanography, I developed new techniques in order to measure the partial molar volumes and conductances of the major salts in seawater with my students.

Wondering about the contrasts between the North Pacific and the North Atlantic, a problem which I reexamine in this publication, I came to the conclusion that making the North Atlantic like the North Pacific would result in a glacial climate. I presented these conjectures in 1966. They were largely confirmed by the subsequent CLIMAP project.

In September 1966 I came to the State University of New York at Stony Brook from which I will retire at the end of this year. For an introductory course in Oceanography, I developed a text-book, published by John Wiley in 1970, and started studying the coastal waters of New York.

As I learned more about the ocean, I began to realize that my original training in "modern physics" was not entirely irrelevant to my current concerns. In utilizing micro paleontological data from the Atlantic to infer the ocean surface climate, relativity of time and space are important. As planktonic organisms drift with the water of the sea, their environment changes due to the change in season and latitudinal drift. Organisms drifting towards the pole in the fall experience rapid cooling whereas, in the same season, a drift towards the equator would entail little change in temperature. To study species distributions in ocean gyres and along drift tracks, one must adopt a relativistic time-space approach.

The variability of the ocean, particularly in coastal areas, introduces a large amount of indeterminacy. Detailed field observations of local coastal waters introduced me to the great time-space variability of the sea. Temporal variations include the regular cycles of the tides and the length of day and the irregular changes of the weather and of river discharge. Spatial

variations result from the interaction of water flow with the complex topography.

Whereas laboratory measurements of the properties of substances can be verified anytime, anywhere, knowledge of the properties of the ever changing sea is limited by the samples taken and the recordings made by in situ instruments. The complexity of oceanographic data was revealed by the quasi continuous measurement of temperature and salinity of subsurface water along the ship's track. These revealed that water properties vary discontinuously. Sudden changes in temperature and salinity occurred because of vertical mixing in the tidal wake of islands. River discharges and heated power plant effluents gave rise to sharp fronts that shifted with the tide. Other peculiarities in the recordings turned out to be artifacts produced by the vessel's seawater plumbing system. It took a while to discover that mysterious spikes on the records were caused by outflow from the sea water surge tank on the vessel, activated by flushing a toilet.

To facilitate coastal zone management, I started developing micro-computer based coastal information systems. The idea was to combine and maintain a geographically specific environmental information system. This would enable potential users of the shore to select sites for specific uses so as to minimize conflicts. A number of preliminary systems were developed for the Port of New York and New Jersey, the Ports of New Orleans and Baltimore and for Chesapeake Bay. Unfortunately, these prototypes did not lead to the establishment of permanent multi-agency systems.

The present preliminary effort is an attempt to synthesize observations about the World Ocean to help envision its behavior.

Chapter one briefly describes uses of the micro-computer to facilitate envisioning of the World Ocean. Envisioning is facilitated by using a square root of depth scale for the vertical coordinate. To map horizontal properties, I use a cartesian chart of the World Ocean, using latitude and longitude in decimal fractions of a degree. To study the continents, one can place Greenwich at the center and run the latitude scale from 160° E, (-200) to 160 °W (+200). To portray the World Ocean one must unite the halves of the Pacific and run the latitudes from 100° W (-100) one to 60° W (+240).

Chapter two deals with the density of seawater. Complications arise from the decrease in the apparent temperature of maximum density with pressure. To deal with this phenomenon which increases thermal expansion with depth, I introduce a **Density Deviation, dD**. It is obtained by computing the in situ density assuming that the pressure in decibars is equal to the

meters, and subtracting a polynomial in Z from the result to reduce the variation with depth.

Chapter three provides an overview of the vertical distribution of the density deviation in the World Ocean using a global set of 21 stations. For most of the stations, the Density deviation converges near a depth of 2704 m (52^2), whereas the temperature and salinity remain apart.

Chapter four examines the density deviation, temperature salinity and dissolved oxygen concentration of the World Ocean at 2704 meters in detail. Some implications of the convergence of density at this depth are examined in Chapter five.

Chapter six examines the contrasts between the North Atlantic and the North Pacific. The apparent paradox that the waters of the saltier ocean, the Atlantic, is diluted by the discharge of 75 percent of the world's largest rivers is explained by the temporary storage of water evaporated from the oceans in river basins.

Chapter seven examines the subtropical gyre of the North Atlantic using the extensive data set from Station "S" south east of Bermuda. By comparing the standard deviation of the density before and after randomizing the temperature - salinity values at the same depth, I show enhanced density sorting at a depth of 600 meters and minima of sorting at 150 and 1000 meters.

I am continuing the task of envisioning the World Ocean and welcome critical comments to help rectify errors of omission or commission in these first seven chapters.

Peter K. Weyl, December 1993

FILE C:\ENV_1\TXT_1

I-1. THE MICRO-COMPUTER AND ENVISIONING

Recent advances in computer science and technology are revolutionizing our ability to access, manipulate and display data. However, the state of the art is still changing rapidly. This is not the time to dwell extensively on optimizing the methodology. Instead I will utilize a variety of generally available techniques to help envision the World Ocean.

To envision, to picture in one's mind, one must communicate aspects of quantitative data to the senses. There are two primary pathways for envisioning, hearing and vision.

Hearing, a sequential process, is primarily useful for envisioning temporal relationships. Numerical data can readily be converted to sequences of sounds, **sonations**, using computers, music software and electronic synthesizers, linked by instructions using the Musical Instrument Digital Interface (MIDI) code.

A serious problem of using sound for envisioning oceanographic data is that time series are seldom continuous. Gaps, sudden intervals of silence, tend to dominate aural perception and thus impede envisioning temporal change.

Sonations may prove useful for envisioning complex relationships between temporal modes of change if the data are without gaps. The primary tools for envisioning, however, are **illustrations**, two dimensional images. The use of spreadsheet microcomputer software greatly facilitates data retrieval, manipulation, display and printing. The illustrations in this document were generated using Quattro® Pro 3.0 software from Borland International Inc.

The World Ocean poses two problems for envisioning its characteristics:

1. Its vertical scale is much smaller than the horizontal ones. If the World Ocean were a square box, its volume of 1.35 E+9 km^3 and area of 360 E+6 km² would have sides 19,000 km in length but a depth of only 3.75 km. A properly scaled profile of the ocean would be a thin line. To resolve variations in the vertical one must greatly exaggerate the vertical dimension.

2. Vertical gradients generally decrease significantly with depth. Typically, the ocean has a surface mixed layer to a depth of about 100 meters. Below this is the main thermocline with steep gradients in temperature and salinity covering several hundred meters. Below the main thermocline

gradients are small until one gets close to the bottom where one can again find steep gradients. The conventional approach is to use separate scales for the surface and the deeper waters. The surface portion may be repeated with the depiction of the entire water column.

A better alternative, facilitated by the use of a spreadsheet program, is the use of the **negative square root** of the depth in meters **-SQRT(Z m)** as the vertical axis. This preserves the vertical order. It provides good resolution for surface gradients and the depth of the mixed near surface layer. It also enhances the progressively smaller gradients with increasing depth. In addition, by exaggerating gradients near the sea floor, the use of the square root emphasizes indications of bottom advection. If depth is displayed as the horizontal (X) axis, the positive square root is used, so that depth increases to the right.

Two Views of Earth
File:C:/MAP/2_WORLDS.WQ1

To map horizontal variations, I use cartesian coordinates of latitude and longitude, entered as decimal fractions of degrees. For global mapping, a crude outline of land areas with a one degree resolution is used. The rectangular map greatly enlarges zonal distances in polar areas. Because of the importance of the polar regions for deep water formation, this distortion is useful.

Fig. I-1.1 shows two depictions of the world, using a Cartesian latitude - longitude grid. The marks at the sides indicate latitudes at 30° intervals and longitudes at 20° intervals. The equator and the 0° and 180° meridians are indicated by dashed lines.

The top map from 160° E to 160° W for a total width of 400° is an appropriate view for envisioning the continents surrounded by the oceans. The bottom map, showing the oceans surrounded by the continents, is more appropriate for displaying properties of the World Ocean. It extends from 100°W on the left, to 60° W in the East, labeled from - 100° to + 320°. Similarly, northern latitudes are positive and southern ones negative.

The bottom view is appropriate for studying the Present World Ocean since the Americas isolate the Atlantic from the Pacific Ocean except for the deep Drake Passage in the South and the shallow Bering Strait in the North. Across the Isthmus of Panama, where the ironies of geography make one travel from West to East to transit the Panama Canal from the Atlantic to the

Fig. I-1.1 Two Views of Earth: a land centered one on top (from 160° E to 160° W) and a World Ocean view below (from 100°W to 60°W).

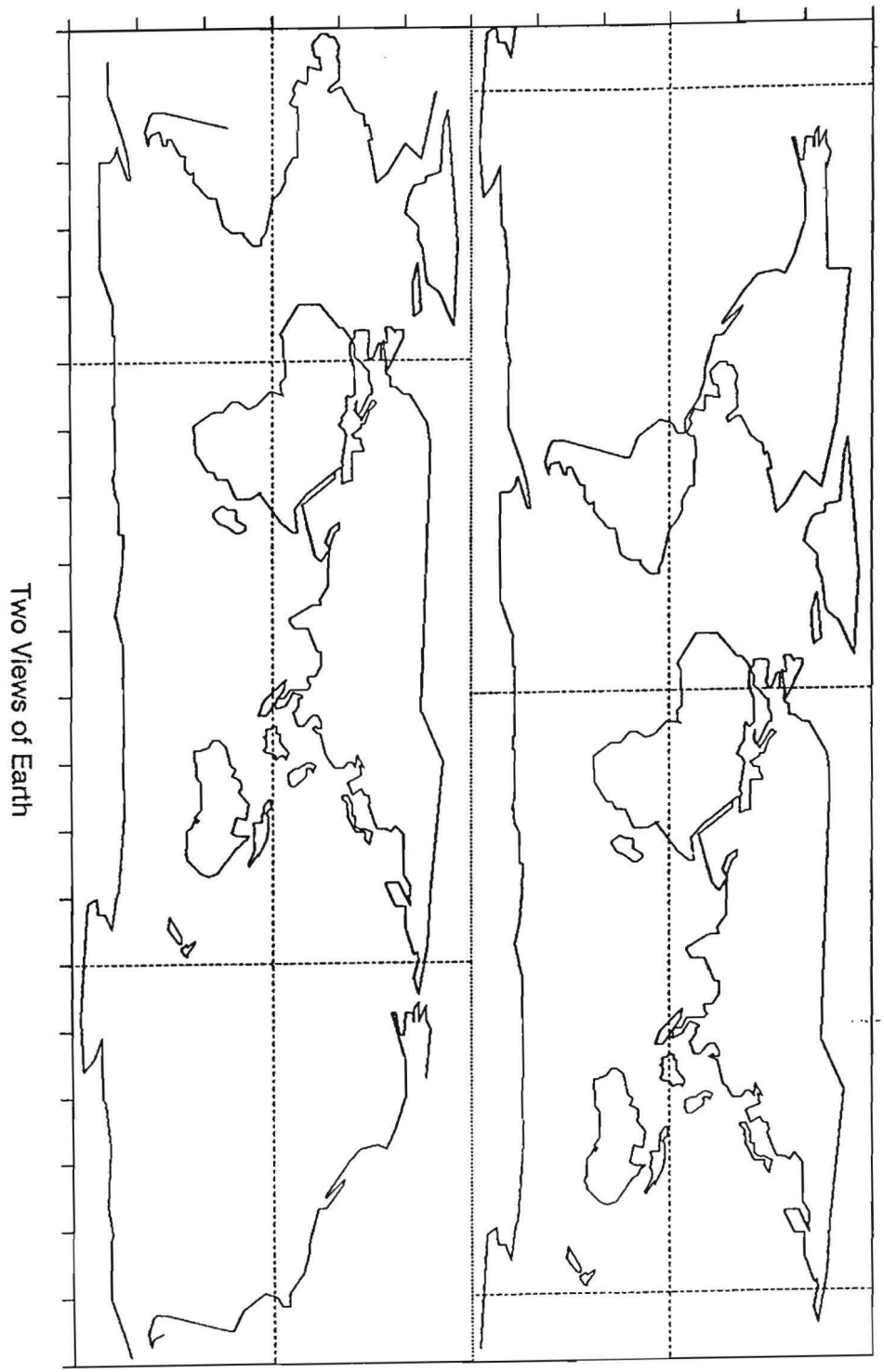

Pacific, the surface waters are over 6 PU (practical units) more saline in the Atlantic than the Pacific. Whereas conventional numbering shows distinct waters to have very similar latitudes and longitudes, this scheme puts them at the extreme west and east. Levitus (1982) in his global statistics of the World Ocean by 5° squares did not not use this scheme so that his squares near Panama merge data from the Atlantic and Pacific. The NODC CD ROM disks organized by 10° squares avoid this problem by segregating the Pacific data on a separate disk. To show continuity through the Drake Passage, it is shown twice at the bottom left and right.

The isolation of the Atlantic from the Pacific has varied. Before about 3 million years ago a seaway across Panama connected the oceans, and the surface waters and biology were not differentiated. When the seaway closed, aggressive terrestrial predators from North America crossed to South America and the salinity contrast across the Isthmus developed. Also, climatic alterations between Interglacial and Glacial periods commenced. During Glacial periods, the lowering of sea level caused by the formation of the continental ice sheets drained the northern connection between the Pacific and Arctic - Atlantic Oceans, the Bering Strait (Weyl 1968).

For Present, Interglacial purposes, however, the lower map provides a suitable outline.

I-2. THE DENSITY OF SEAWATER

The laws of motion depend only on the density of seawater, not on the three separate variables, the temperature, salinity and pressure. At the sea surface, the ocean loses heat by evaporation, infrared radiation and the sensible transfer of heat to the atmosphere. The ocean gains heat by the absorption of short wave radiation in the illuminated surface layer and by condensation. The downward penetration of visible shortwave radiation, combined with heat loss exclusively at the surface, results in a near surface mixed layer, whose thickness varies with the seasons.

As water sinks below the surface, its density increases as a result of the increase in pressure. Adiabatic compression also increases its temperature, slightly decreasing the density. If the density of seawater D(T,S,P) could be expressed in terms of three functions **A**(T,S), B(P) and **C**(P), such that: D(T,S,P) = **A**(T,S)*B(P) + **C**(P), then, to study the thermo-haline properties of seawater **A**(T,S) one could ignore the pressure terms **B** and **C**. If the effect of pressure were exclusively the change in temperature due to adiabatic compression, then A(θ,S) where θ is the potential temperature corresponding to T and P would provide an adequate description of **relative** density relationships in the World Ocean.

But that is not the case, primarily because pure water at atmospheric pressure has a temperature of maximum density at 4° C. The temperature of maximum density decreases with the addition of sea salt approximately by one degree Celsius per about 4.5 PU increase in salinity. More important for the physical behavior of the World Ocean is the decrease of the temperature of maximum density with increasing pressure at a rate of about 1° C per 450 decibars.

As a result, thermal expansion, particularly at low temperatures, increases significantly with increasing pressure. Thus the effect of pressure can not be separated from the thermo-haline terms. Since the partial density of sea salt is much larger than that of water, salinity only contributes slightly to the non-linear behavior by lowering the temperature of maximum density.

The effect of the lowering of the virtual temperature of maximum density is illustrated in **Fig. I-2.1.** It shows the adiabatic lapse rate (ALR) and the change in density (dD/dT) with pressure as a function of temperatures for pressures of 0, 1000, 2000, 3000, 4000 and 5000 decibars.

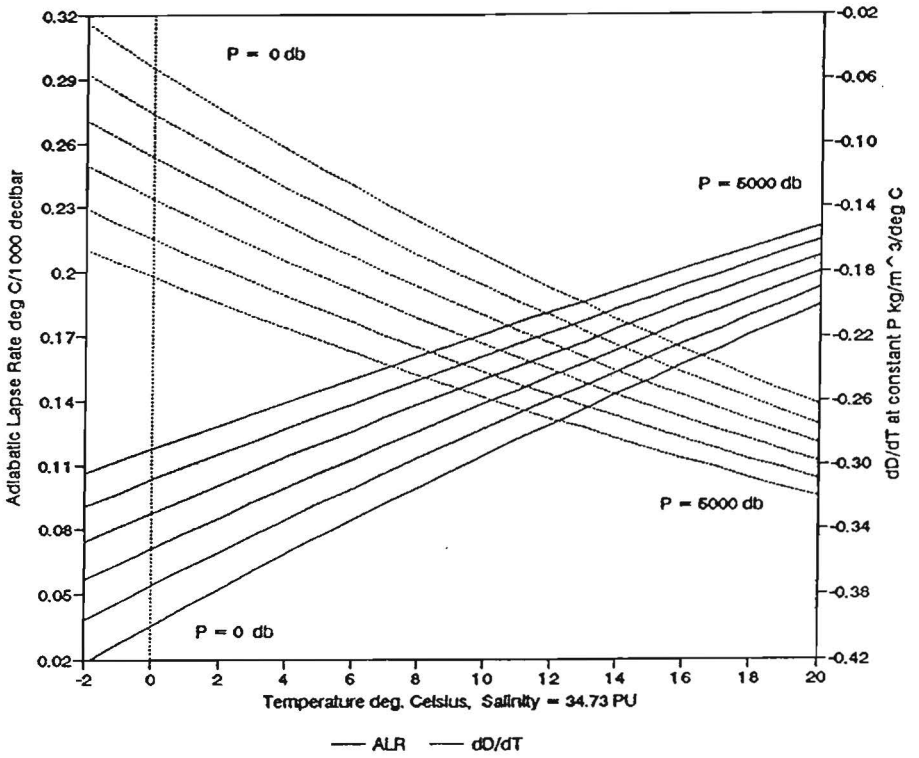

Fig.I-2.1 The Adiabatic Lapse Rate (ALR) in degrees Celsius per 1000 decibar and the change in density in kg/m^3 per degree Celsius for (dD/dT) seawater with salinity 34.73 PU as a function of temperature and pressure.

The adiabatic lapse rate is a minimum at the sea surface at low temperatures and increases with temperature and pressure. However, its pressure dependence is greatest at low temperatures. The rate of decrease of density with increasing temperature is also a minimum at low temperatures and pressures and increases with increasing temperature and pressure. In both cases, the effects are greatest at low temperatures and pressures, when the virtual temperature of maximum density is at a maximum. Between -2 and 20 °C the lapse rate increases by about a factor of ten and thermal expansion increases by slightly more.

If one assumes that the temperature and salinity of seawater are only modified at the sea surface, then salinity and potential temperature are invariant. The properties of surface waters, however, tend to be patchy, differing in temperature, salinity and density. With depth, the variability declines for the following reasons:

1. Because the equation of state of seawater at constant pressure is not linear, mixtures of water of equal density but differing in temperature and salinity become denser after mixing.

2. As waters of equal density at a fixed pressure, but differing in temperature and salinity are displaced vertically by waves, their density relationships also oscillate, inducing intense vertical mixing. With increasing pressure, the warmer saltier water becomes less dense, while the cooler fresher water becomes denser. This effect is reinforced by the increase in the adiabatic lapse rate with temperature.

The density of seawater is a function of temperature, salinity and pressure. However, oceanographic data is tabulated as a function of depth rather than pressure. To determine the pressure, one must integrate the acceleration of gravity, which varies with latitude and depth, times the density from the surface to the desired depth. However, the pressure in the sea in decibars is approximately equal to the depth in meters. Further, the ratios of adjacent pressures will be close to the ratios of the corresponding depths. I use the equation of state for seawater of Fofonoff (1985) but replace the pressure in decibars by the depth in meters.

To permit density comparisons over wide depth ranges, I introduce a **Density Deviation (dD)** that is obtained by subtracting a polynomial of the depth in meters from the value of SigmaT(T,S,Z), Equation 2-1.

Eq.I-2.1 $dD = SigmaT(T, S, Z) + A0 + Z * A1 + Z^2 * A2$

$A0 = -27.4$, $A1 = -4.79$ E-3, $A2 = +5.7$ E-8

The coefficients (Ai) in equation 2-1 have been chosen so that the vertical gradients in **dD** in deep ocean water are generally small. As I will show in a subsequent section, the Density Deviation for World Ocean waters at a depth of 2704 meters (52^2), not isolated by sills of lesser depth, is virtually constant between 65° North and 55° South with an average value of 0.2 kg/m^3.

Plots of the density deviation as a function of depth permit comparisons of densities between stations at the same depth. Since the empirical coefficients in equation I-2.1 reduce the vertical gradients in density below the main thermocline, one can readily compare density deviations over extended depth ranges.

To relate the slope of the density deviation to that due to adiabatic displacement at a specific depth, one can add adiabatic segments to the density deviation curve. An example of this is **Fig. I-2.2**, which uses STD data for the TTO-Tropical Atlantic (Cruise # 9853), Station # 114 at the equator and 28.0° West. In addition to the density deviation, the salinity is also shown as a heavy dotted line. the salinity minimum of the Antarctic Intermediate water at 784 m is about 34.50 PU and the salinity maximum of the North Atlantic Deep Water at about 1800 m is 34.98 PU.

To indicate the slope that would result from adiabatic vertical displacement, I selected 8 observations distributed over the depth range. For each observation, I compute -SQRT(Z) = ±2 and obtain the corresponding value of Z. I compute the adiabatic gradient using the equation of Bryden H.L. (1973) and determine the temperature of the water after displacement. Next, I calculate the density deviation for SQRT(Z ±2) at the observed salinity and the temperatures along the adiabatic curve. The short line segments are then superposed on the density deviation curves using a separate Y axis with dotted lines.

Note that the adiabatic curves are almost normal to the density deviation curves and become almost coincident near the bottom of the graph. In the upper part there are several almost stepwise changes in the density deviation curve that approach the slope of the adiabatic lines.

Fig. I-2.2 TTO Station #114, Density deviation and salinity as a function of the depth S min = 34.50 PU, Smax = 34.98 PU, Line segments correspond to the density deviations resulting from vertical adiabatic displacements of ±2 in SQRT(Z).

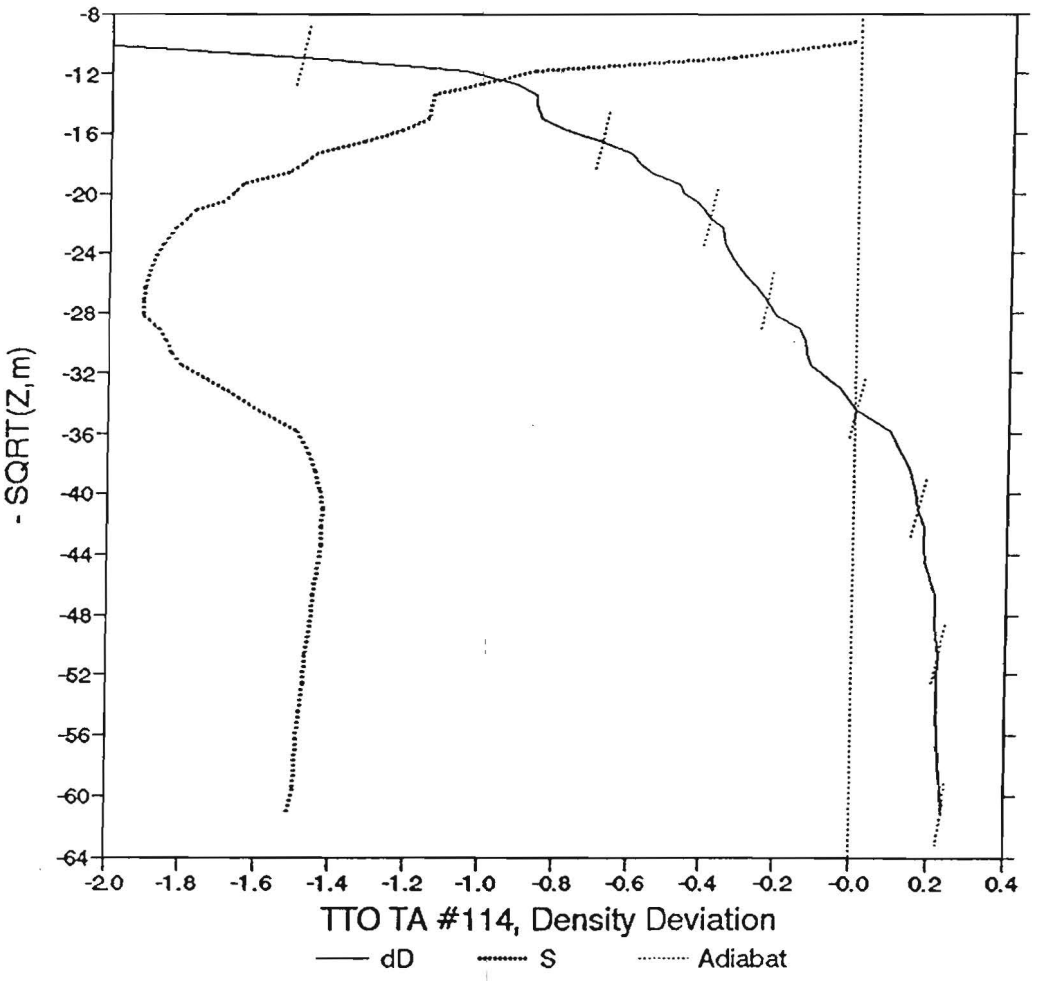

I-3. THE WORLD OCEAN, AN OVERVIEW

To provide an overview of the **vertical density structure** of the World Ocean I examine a set of 21 Stations , A - X, listed in **Table I-3.1** ,whose positions were shown in **Fig. 3-1.**

Table I-3.1 Stations used:

		Index of stations in WO sets								Ty
Label		Ocn	Lat	Lat3	Long	YY	MM	DD	Ves	Obs
A		Arctic Oce	82.7		158.3	63	7	12	31T3	22 1
B	GSX	Greenland-	74.9		-1.1	72	8	18	316N	67 2
C	GSX	Atl	51.0		-43.0	72	7	27	316N	70 2
D	GSX	Atl	36.0		-68.0	73	3	30	316N	71 2
E	GSX	Atl	28.0		-26.0	73	3	15	316N	51 2
F	GSX	Atl	15.0		-53.9	72	10	11	316N	74 2
G	GSX	Atl	-39.1		-48.6	72	12	5	316N	76 2
H	33		-43.1		-30.3	31	4	22	74DS	23 1
I	GSX	Ind	4.0		56.8	78	1	8	318M	72 2
J	GSX	Ind	12.5		84.5	78	3	28	318M	64 2
K	40		-42.1		70.7	60	12	21	31AR	32 1
L	GSX	Pac	53.1		182.7	73	10	8	318M	66 2
M	GSX	Pac	34.3		142.0	73	10	24	318M	79 2
N	GSX	Pac	34.2		232.1	73	8	25	318M	71 2
O	10	Scorpio	-43.3		152.1	67	3	13	31ET	38 1
P	13	Scorpio	-43.2		220.8	67	4	14	31ET	39 1
Q	14	Scorpio	-43.7		260.0	67	4	28	31ET	36 1
T		Ross S	-75.0		165.6	78	2	7	31BI	53 2
X	GSX	Atl	-61.1		-63.0	73	1	3	316N	73 2
X	GSX	Atl	-61.1		297.0	73	1	3	316N	73 2
Y		Southern O	-61.0		-1.2	86	7	19	06AQ	79 2

Fig. I-3.2 shows the vertical **density deviation dD** for the stations for values of the negative square root of the depth ranging from 0 to -75. Near the surface, the density deviation ranges from -6 to +0.6 kg/m^3. With depth, the density deviation curves converge rapidly so that the overall range is less than 1 kg/m^3 below -SQRT(Z) less than -35.

The variations in dD are seen in more detail in **Fig. I-3.3** where the density scale has been expanded. Note that for -SQRT(Z) between -48 and -55, the density difference for most of the World Ocean has a range of less than 0.1 kg/m^3.

Fig. I-3.1 Map of the Overview stations

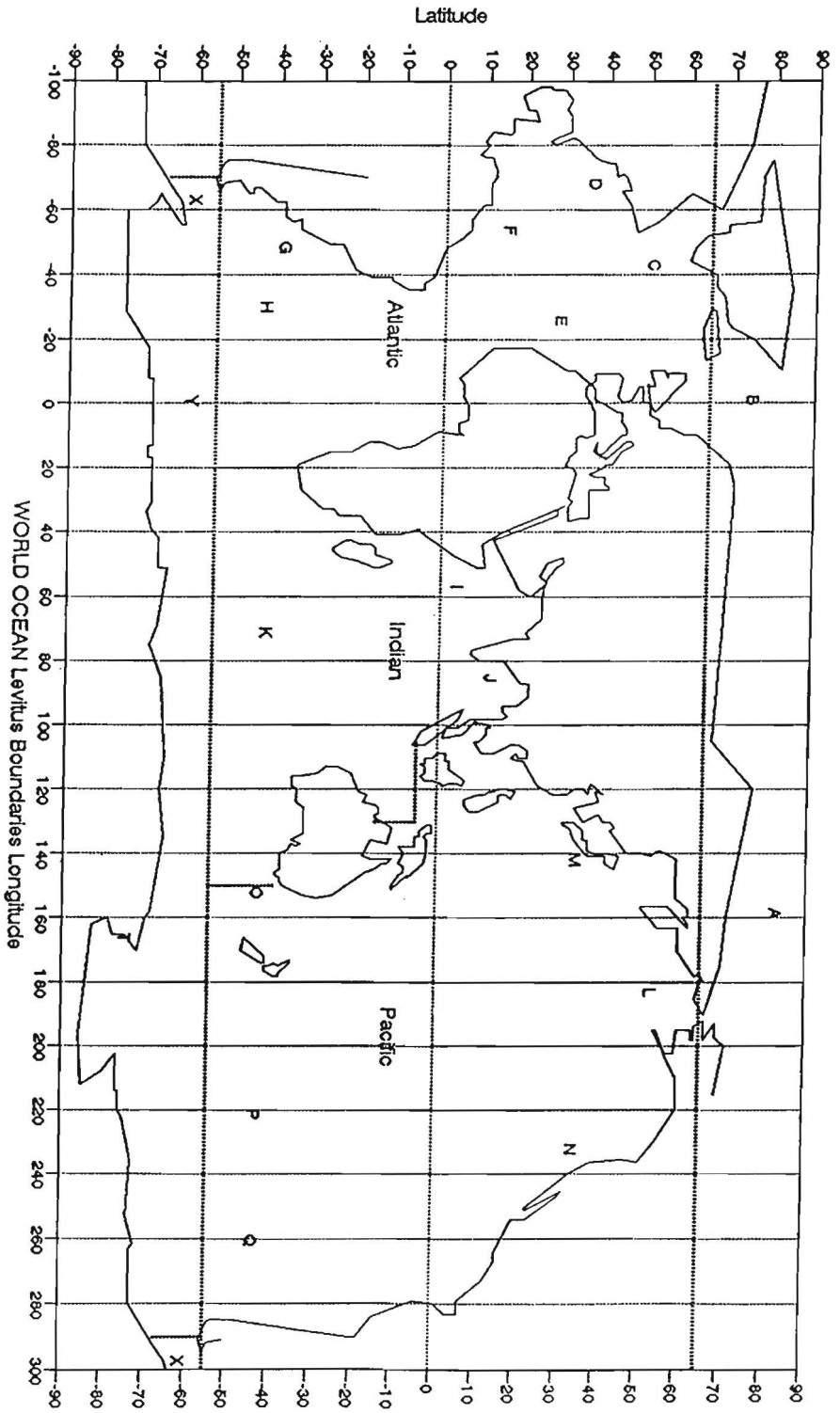

Fig I-3.2 Density Deviation as a function of depth for the Overview stations.

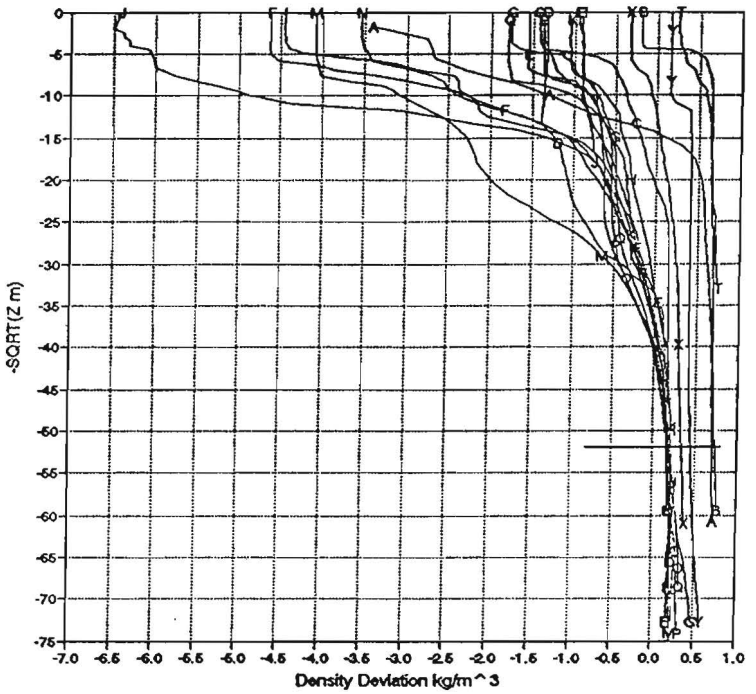

Fig. I-3.3 Same as Fig I-3.1 but expanded density scale.

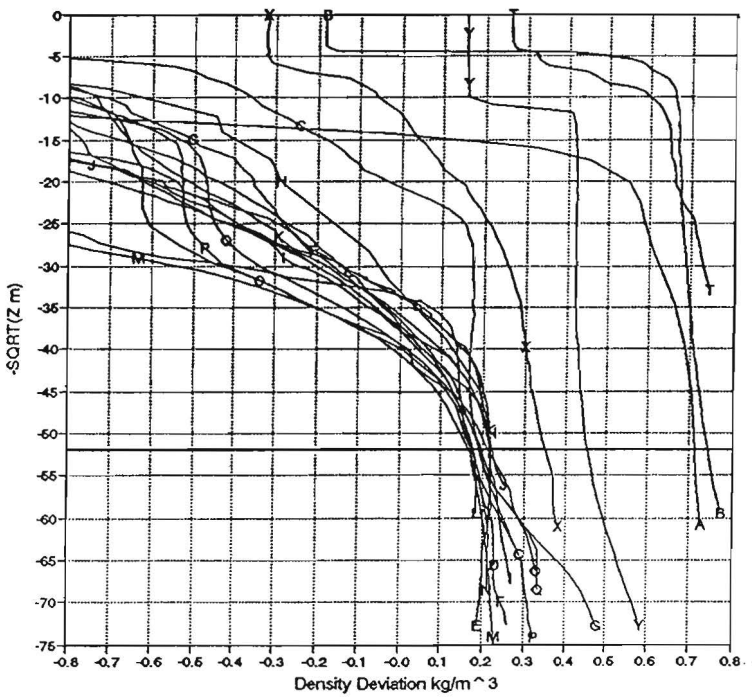

Stations with significantly higher densities at depth are: stations A and B in the Arctic Ocean and in the adjacent Greenland Norwegian Sea and X, Y and T south of 60° South near the Antarctic continent. The high density of the deep waters at stations A and B result from the isolation of these waters by sills. In contrast, the dense waters near Antarctica are dynamically isolated by the interaction of current gyres with the rotation of Earth.

The close correspondence in the density deviation between the relatively isolated North Atlantic and North Pacific are remarkable. Note that the density differences (Fig. I-3.3) diverge somewhat towards the bottom for -SQRT(Z) less than -60 as a result of the deep advection of waters from the polar regions.

Figures **I-3.4** and **I-3.5** give the vertical variations in salinity and temperature for the same stations. They show that the uniformity in the density deviation near SQRT(Z) = 52 is the result of compensating variations in T and S. The warmer, saltier waters of the North Atlantic and North Indian Oceans contrast with the colder less saline waters of the North Pacific.

A temperature - salinity diagram for the stations is shown in figure **I-3.6**. Because of the large range in pressure, the lower temperature portion of this diagram (below about 5° C) is not very informative.

To study the homogeneity of the density deviation in more detail, I next look at the global distribution of properties at the 2704 meter (SQRT(Z) = 52) depth level, using data from GEOSECS, supplemented by severeal TTO stations.

Fig. I-3.4 Salinity as a function of depth for the overview stations.

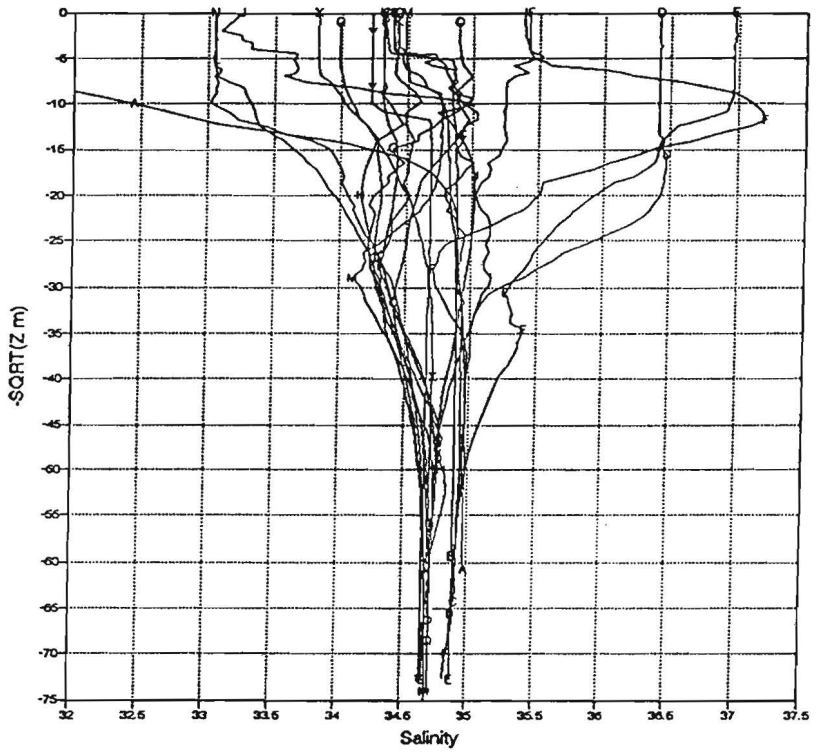

Fig. I-3.5 Temperature as a function of depth for the overview stations.

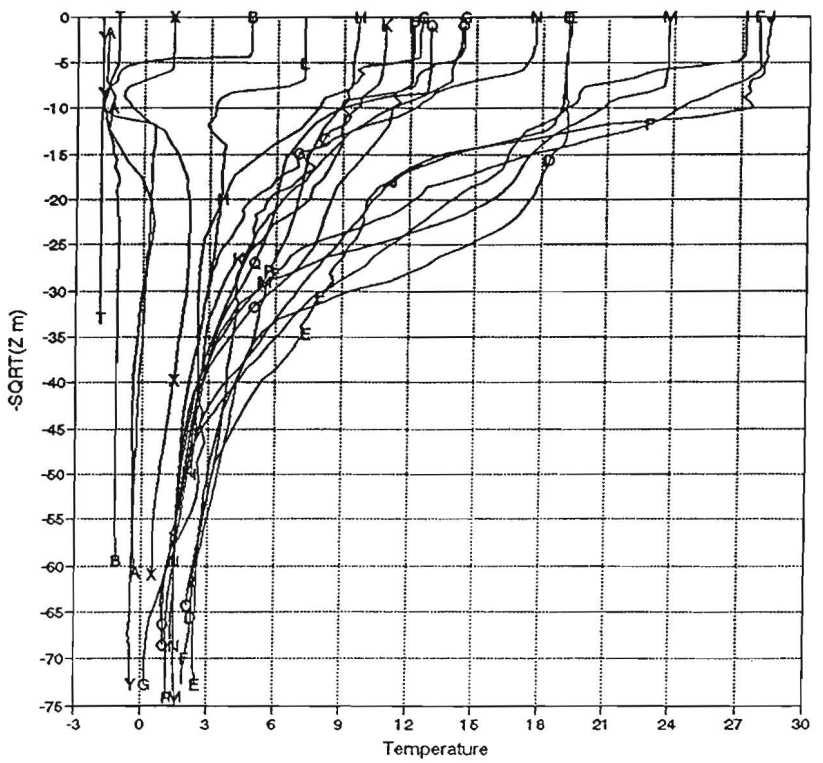

Fig. I-3.6 Temperature - Salinity diagram for the overview stations.

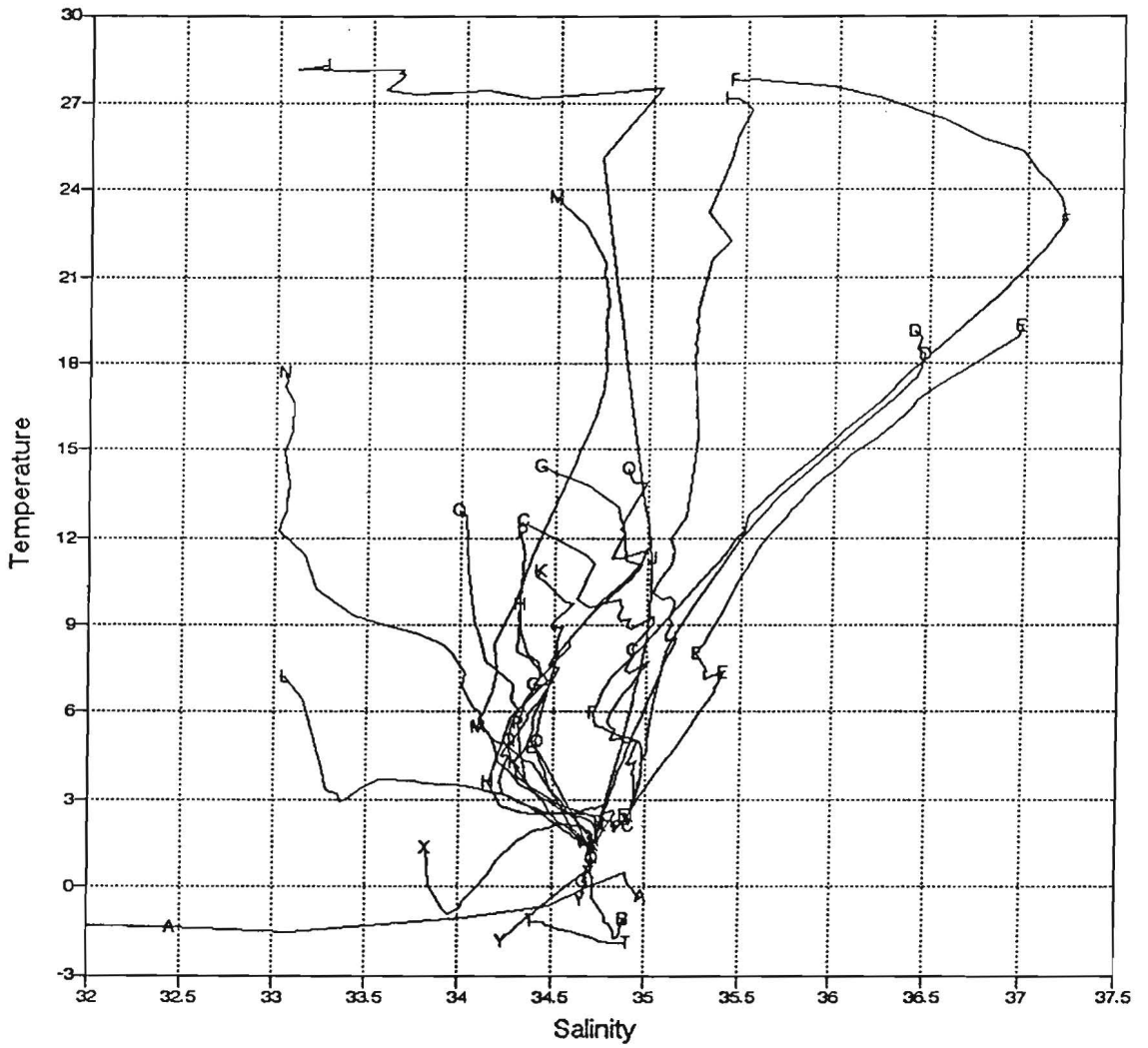

I-4. THE WORLD OCEAN AT 2704 meters
File:C:\ENV_1\Q52_GSX.WQ1

Section I-3 suggests that for most of the World Ocean, the density deviation at 2704 meters shows little variation. At this depth, the waters of the three major ocean basins, the Atlantic, Indian and Pacific, are interconnected by the Southern Ocean and the Mid-Ocean Ridges only offer intermittent blockage.

To verify that the density deviation, **dD** near 2704 meters is essentially constant over much of the World Ocean, let us examine data from the GEOSECS expeditions covering the Atlantic, Pacific and Indian Oceans, supplemented by Atlantic data from the TTO North Atlantic and Tropical Atlantic cruises. The published data were linearly interpolated to estimate parameters at 2704 meters depth.

Fig. I-4.1 is a temperature salinity diagram of the interpolated data at 2704 meters. The heavy line represents a constant density deviation **dD = 0.2**, a SigmaT(T,S,p=2704 db) value of 40.135 kg/m^3. Most station data are represented by **+**. The warmest data, point **C** is from the isolated waters of the Caribbean (TTO Trop Atl. #4). The high density, low temperature and high salinity points **a** are from north of the Greenland- Iceland-Shetland Ridge.

Points **X** are from the TTO North Atlantic Expedition stations 166 and 171 where the 2704 m level is close to the bottom. The near bottom water is a mixture from the overflow of dense waters across the Denmark Strait between Greenland and Iceland and North Atlantic water. Point **A** corresponds to the characteristics of Antarctic Bottom water, lowered adiabatically to a pressure of 2704 db (S = 34.66, Pot T = -0.8 °C).

Most data fall close to the heavy line corresponding to **dD = 0.2**. The points near the dashed line are from the Southern Ocean, close to the Antarctic Continent.

Fig. I-4.2 shows the salinity as a function of the density deviation for the same data.

To display the spatial distributions of properties at 2704 meters I divide the cartesian coordinates of the World Ocean Chart into 2.5° latitude by 5° Longitude pixels. If more than one station falls into a pixel, their values are averaged. Each pixel is large enough to display a two digit integer.

Fig. I-4.1 Temperature - Salinity Diagram at 2704 m.

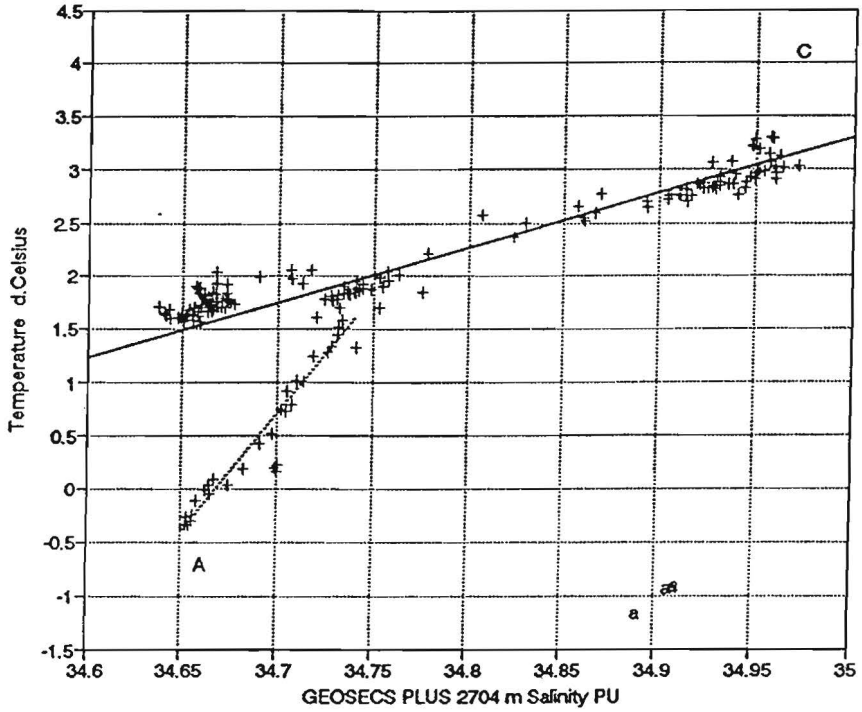

Fig. I-4.2 Density Deviation- Salinity Diagram at 2704 m.

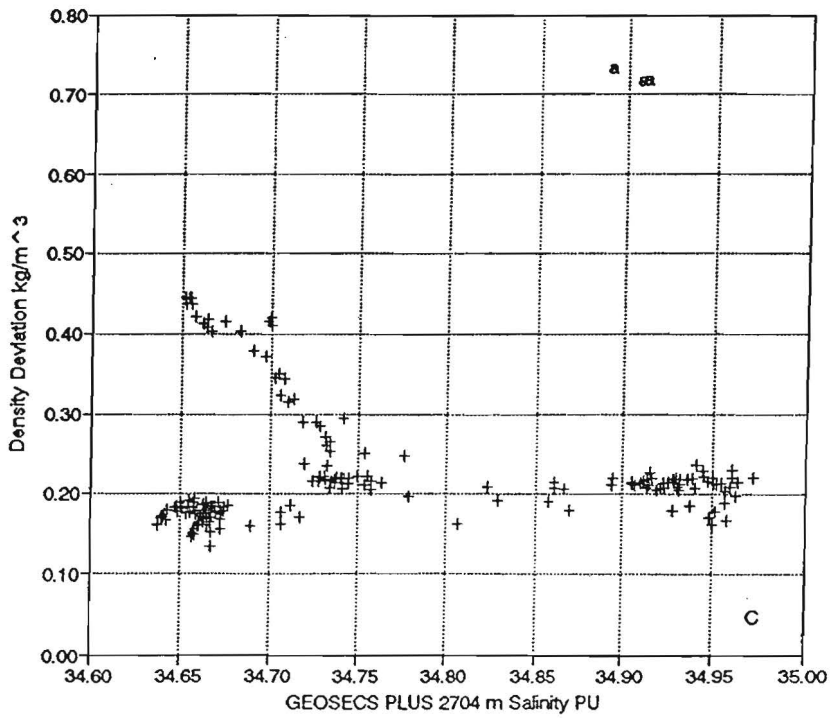

The maximum and minimum observed values of a parameter for the parts of the World Ocean not isolated by sills of lesser depth are assigned values of 100 and 0 respectively. In the case of the density deviation, they correspond to values of dD of .136 and .449 kg/m^3 respectively, a range of 0.312 SigmaT units.

The resulting global distribution of the density deviation dD is shown in **Fig. I-4.3.** The percent density deviation ranges from 220 for the Mediterranean, 192 in the Greenland-Iceland-Norway Sea to -28 in the Caribbean Sea. In the connected part of the World Ocean, the highest density deviations at 2704 meters were observed in the Southern Ocean and the least dense waters in the Pacific,(0 at 47° S, 190° E and 1 at 55°N, 167°E). The overall range in density deviation of the connected part outside the Southern Ocean only ranges from 0 to 30 percent, corresponding to dD values between 0.136 and 0.230, a range of less than 0.1 kg/m^3. Thus the data confirm the interpretation of the limited "Overview" data that horizontal density gradients near 2704 meters are small, except for Antarctic waters and isolated basins.

Fig. I-4.4 shows the spatial distribution of salinity based on the same data set. A value of 0 percent corresponds to a salinity of 34.637 PU and 100 percent corresponds to a salinity of 34.972 PU. Notice that the salinity increases from South to North in the Atlantic and Indian Oceans with low values near the Antarctic continent. In contrast, the salinity decreases towards the North in the Pacific with the highest values, 29 percent, 34.73 PU occurring near 55° S, South East off New Zealand. The North Atlantic is the dominant source of high salinity deep water with a lesser source in the North Indian Ocean. In contrast, the deep water originating near Antarctica is much less salty.

Since dissolved oxygen can be added only near the sea surface by solution of atmospheric oxygen and photosynthesis using sunlight whereas respiration occurs at all depths, the concentration of dissolved oxygen at 2704 meters gives an indication of the "age" of the water, the time since it was at or near the sea surface. The distribution of dissolved oxygen is shown as a percentage of its range in **Fig. I-4.5.** The range 0 to 100 corresponds to values from 82 to 321 uM/kg of dissolved oxygen in seawater.

High concentrations of dissolved oxygen at 2704 meters occur in the Atlantic sector with the highest values in the Arctic region. The increase in oxygen South of about 55°S indicates ventilation of the deep near Antarctica. In the Indian and the Pacific sectors, the concentration of dissolved oxygen decreases towards the north, with the lowest values in the North Pacific.

Fig. I-4.3 Density Deviation at 2704 m in percent;
0 = .136, 100 = .449 kg/m^3.

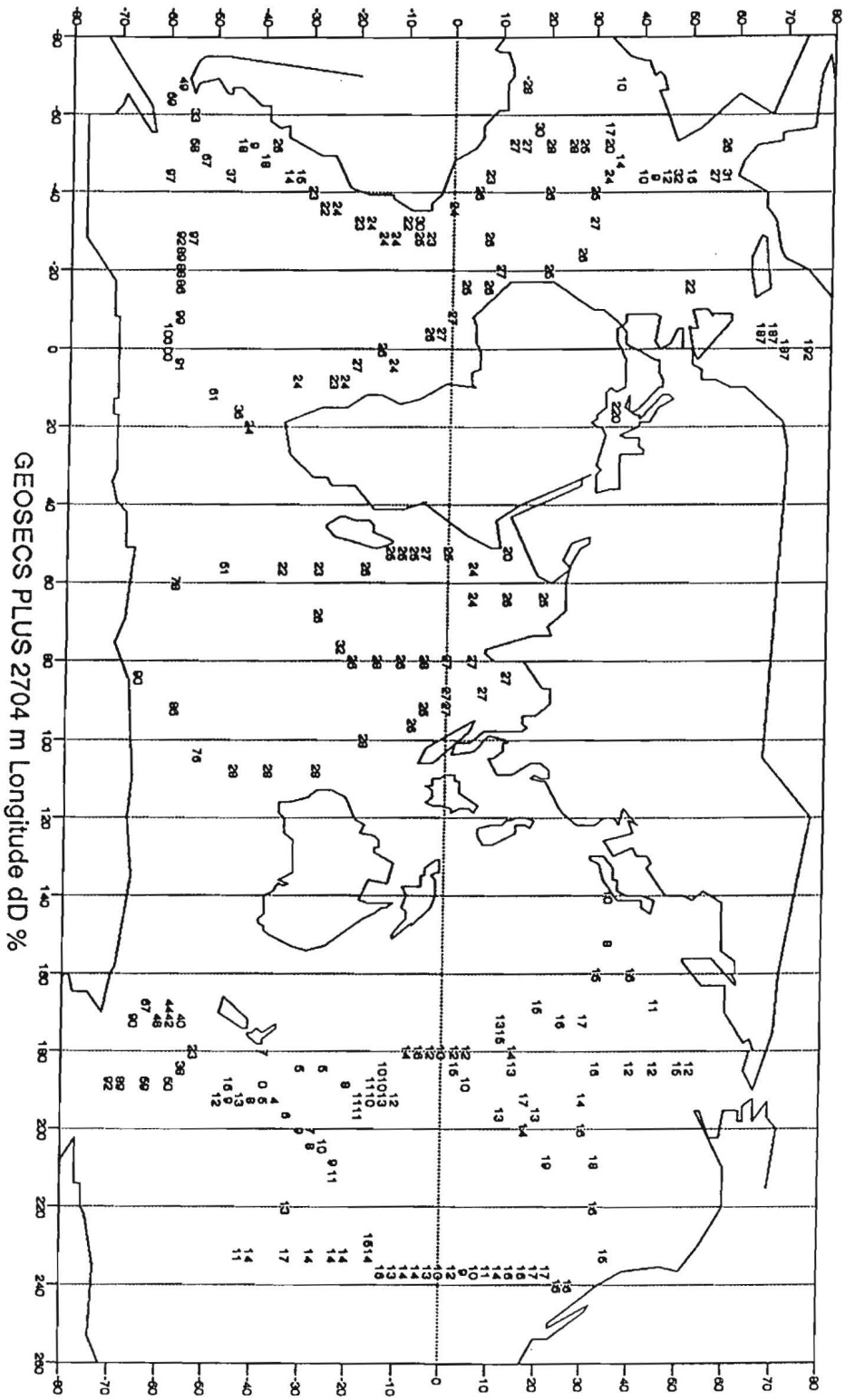

Fig. I-4.4 Salinity at 2704 m in percent;
0 = 34.637, 100 = 34.972.

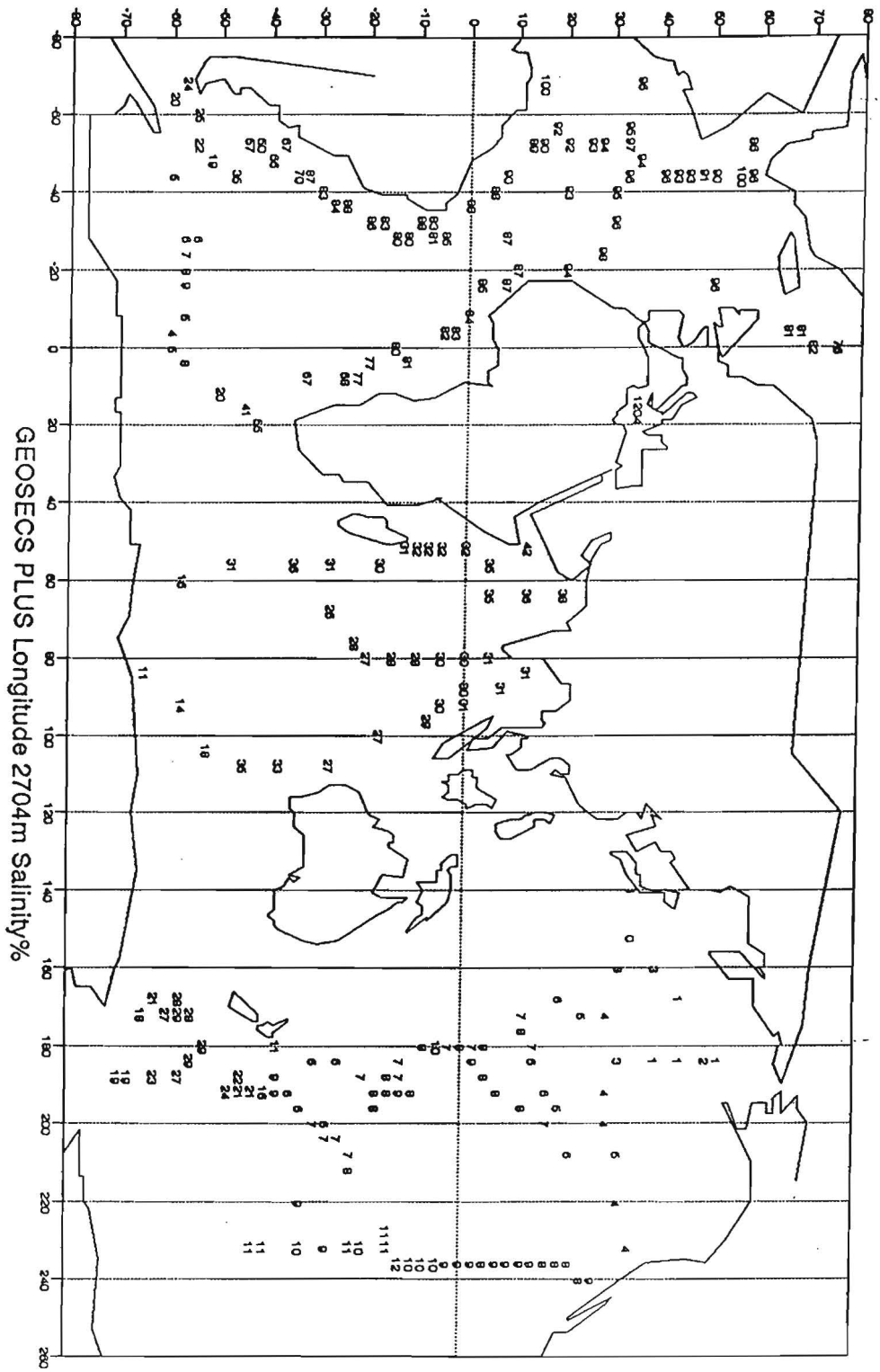

Fig. I-4.5 Concentration of Dissolved Oxygen at 2704 m in percent; 0 = 82, 100 = 281 uM/kg.

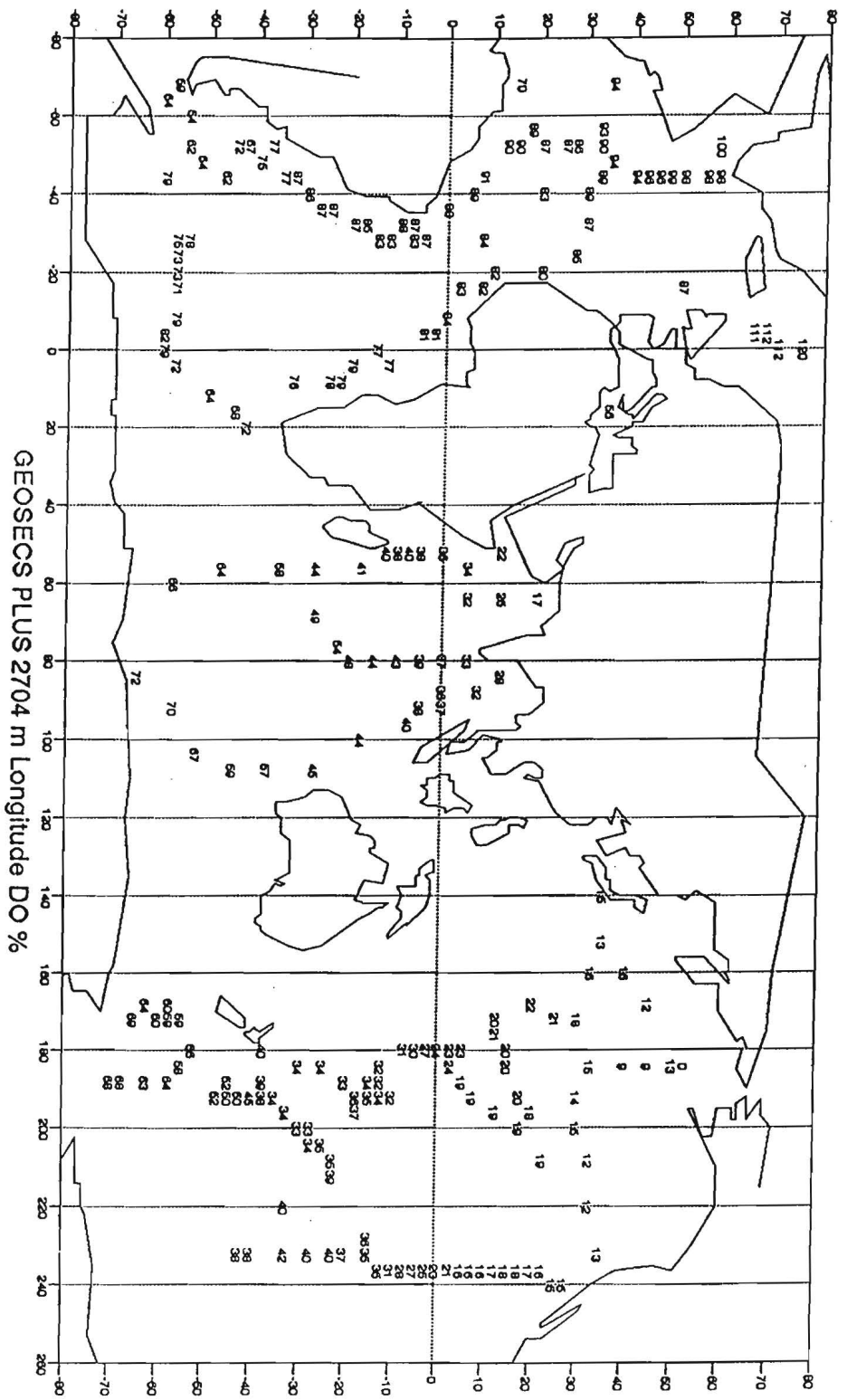

In calculating the density deviation I use the depth of the observation in meters rather than the pressure in decibars. To what extent does this approximation invalidate the conclusion that the densities at 2704 meters are essentially constant? As a test, I compared calculations from the very different waters in the North Atlantic and North Pacific, using both the depth and the pressure as recorded in the GEOSECS Hydrographic Data volumes to calculate the density deviation. The results are shown below:

Area	Stn#	Zm	Pdb	T°C	S PU	dD(Z)	dD(P)	Error
NEA	115	2704	2738	3.033	34.964	0.216	0.214	+.002
NWA	121	2704	2739	3.089	34.958	0.203	0.200	+.003
NEP	201	2704	2738	1.655	34.652	0.182	0.181	+.001
NWP	224	2704	2737	1.701	34.642	0.167	0.167	.000

The pressure in decibars is approximately 35 units larger than the depth in meters and so the density calculated when using the depth is smaller. However, the empirical polynomial used in calculating the density deviation slightly overcompensates for the discrepancy resulting in a slightly greater "density" difference, primarily in the Atlantic. Therefore the use of depth instead of pressure is justified for comparing densities at this level.

CONCLUSIONS

1. The density deviation at 2704 meters and therefore the in situ density at this depth varies little in the connected parts of the World Ocean between about 55° S and 65° N.

2. Significant input of dense, oxygenated water occurs in the North primarily by overflow from the Greenland-Iceland-Norway Sea and sinking in the extreme NW Atlantic and in the Southern Ocean near Antarctica.

3. The dominant sources of deep high salinity water is in the North Atlantic. A minor source is the North Indian Ocean.

4. Ventilation, the addition of dissolved oxygen at 2704 meters is limited to the Far North Atlantic and the region around Antarctica. In the Indian and Pacific Oceans, the oxygen concentration decreases towards the North.

5. Conservation of mass requires that the down welling of dense oxygenated water North of about 65°N in the Atlantic and South of about 55°S in the Southern Ocean, across the 2704 m surface be balanced by upwelling elsewhere.

6. The use of depth rather than pressure does not introduce significant error in comparing densities at this level.

7. The density deviation at 2704 m as calculated using equation I-2.1 approximates the true in-situ density difference to better than 0.01 kg/m^3.

I-5 IMPLICATIONS

In section I-4 I showed that between about 55° South and 65° North, the World Ocean at 2704 m depth has a density deviation close to 0.2 kg/m^3. **Table I-5.1** summarizes data on the areas and volumes of the World Ocean relative to the 2704 meters level.

Table I-5.1

Ocean	Area E+6 km² at 2704	Volume E+6 km^3 below	Avg thickness meters	Volume E+6 km^3 above
65N to 55 S				
Atlantic	61.0	102.0	1670	164.9
Indian	52.5	79.9	1520	142.0
Pacific	135.9	269.5	1980	367.5
Total	249.3	451.4	1810	674.4
N of 65N	2.6	2.0	770	7.0
S of 55S	26.6	46.1	1730	71.9
World Ocean	279	500		752

Data derived from Levitus 1982

Of the 1,250 E+6 km^3 volume of the World Ocean between 65° N and 55° S deeper than 2704 meters, about 450 E+6 km^3 or 36 percent falls below the 2704 meter level. If one assumes that the average residence time of this water is 1000 years, renewal requires an annual input of 450 E+3 km^3, a flux of 14 Sverdrups. This downward flux must be balanced by an average annual upward displacement of 1.8 meters/year.

If sinking takes place south of 55° S and North of 65° N, and upwelling between these latitudes, a residence time of 1000 years would require an average upward velocity of about 2 meters per year. The average density difference between the downwelling and the upwelling water would be about 0.2 kg/m^3. At 2704 meters, the Northern water has a density deviation of 0.45 and a salinity of about 35 PU and the southern water has a density deviation of about 0.40 and a salinity of about 34.68. The water that wells up across 2704 m, however, has a density deviation of about 0.18. Per year, the density of a 2 meter layer of water would have to be reduced by more than 0.22 kg/m^3.

The average geothermal heat flux amounts to about 44 cal/cm^2 yr. This is sufficient to heat the 1.8 m of water by 44/180 = 0.24°C and reduce the density by about 0.03 kg/m^3, about 14 percent of the required amount. The rest of the density reduction would have to occur by vertical mixing across the 2704 meter surface.

6. THE NORTH ATLANTIC NORTH PACIFIC CONTRAST
C:\ENV_2\TXT_2

I have demonstrated that the density of the World Ocean at 2704 meters depth is essentially constant, between 65° N and 55° S. What differentiates the northern oceans, however, is that the North Atlantic is saltier and warmer than the North Pacific. The volumetric average properties of the ocean basins, as determined by Levitus (1982), reveal the following North Atlantic - North Pacific differences:

Property	N Atl. - N Pac.	Difference	
Potential Temperature	4.87 - 3.44 =	**+0.63**	°C
Salinity	35.12 - 34.58 =	**+0.54**	PU,
Dissolved Oxygen	5.29 - 2.56 =	**+2.73**	ml/l.

The salinity - temperature contrast is greatest in the two subtropical anticyclonic gyres, located roughly between latitudes 20° and 40° North.

To show the contrast in more detail, **Fig. I-6.1** (N_STGYR.WQ1) compares the temperatures and salinities of the two gyres, using vertical STD sections from the GEOSECS expeditions. The Stations are:

Atlantic # **30**, 31.8° N, 50.8° W 9/20/1972;
Atlantic # **120**, 33.3° N, 56.6° W 3/27/1973;
Pacific # **226**, 30.6° N, 170.6° E 11/09/1973.

In March, (Stn.120), the depth of the mixed layer is significantly deeper and the temperature lower (18°) than in September (Stn. 30). The surface North Pacific salinity is about 1.4 PU less than that of the Atlantic stations and at 900 meter depth in the Atlantic, the salinity is still greater than the surface salinity in the Pacific. Note that the salinity minimum at 625 meters, the result of the intrusion of North Pacific Intermediate Water, has no counterpart in the Atlantic.

The density deviations for the same stations are compared in **Fig. I-6.2**. Below the seasonally warmed layer (144 m depth), the two Atlantic stations have virtually the same density. The Pacific station remains less dense, however; that difference is reduced below about 400 meters.

Fig. I-6.1 Temperature and Salinity as a function of depth for stations from the Subtropical Anticyclonic Gyres of the North Atlantic and North Pacific (GEOSECS 30,120 and 226).

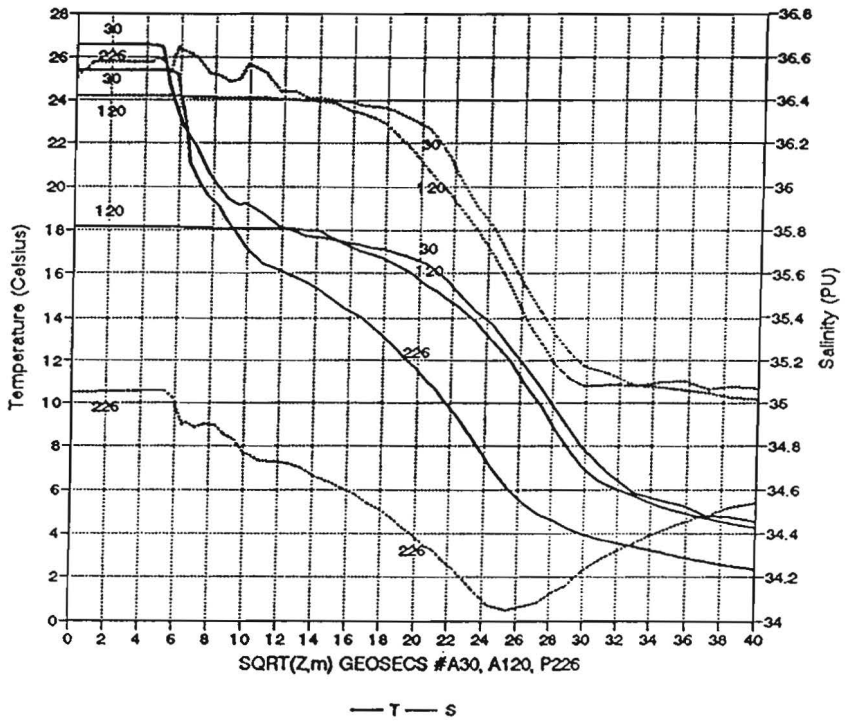

Fig. I-6.2 Density Deviation in kg/m^3 function of depth for stations from the Subtropical Anticyclonic Gyres of the North Atlantic and North Pacific (GEOSECS 30,120 and 226).

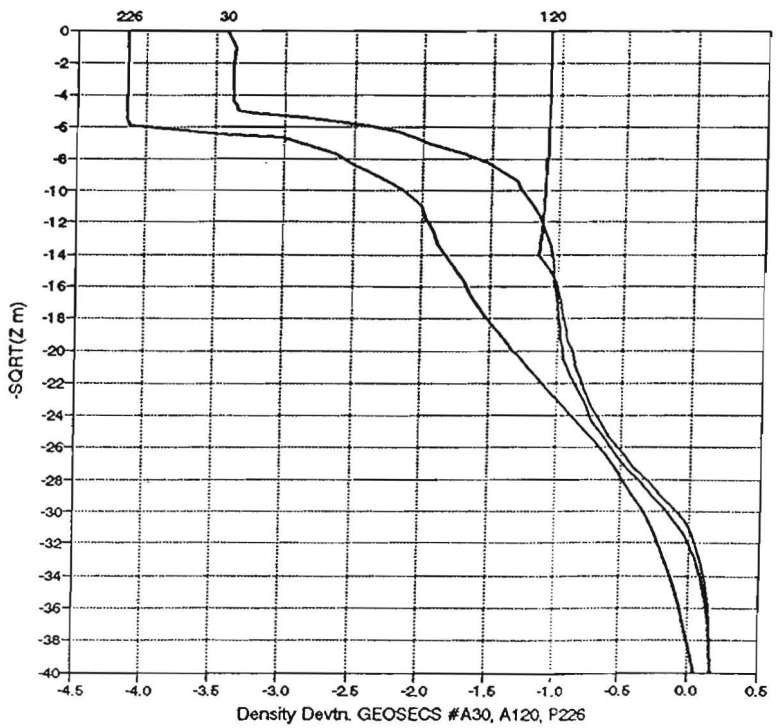

The Temperature - Salinity curves for the three stations are compared in **Fig. I-6.3.** Between 18° and 8°, the temperature and the salinity both decrease with depth. However, the slope dS/dT in PU/°C is almost twice as large (1.3/0.7) in the North Atlantic as in the North Pacific.

Fig. I-6.3 Temperature - Salinity diagram for stations from the Subtropical Anticyclonic Gyres of the North Atlantic and North Pacific (GEOSECS 30,120 and 226).

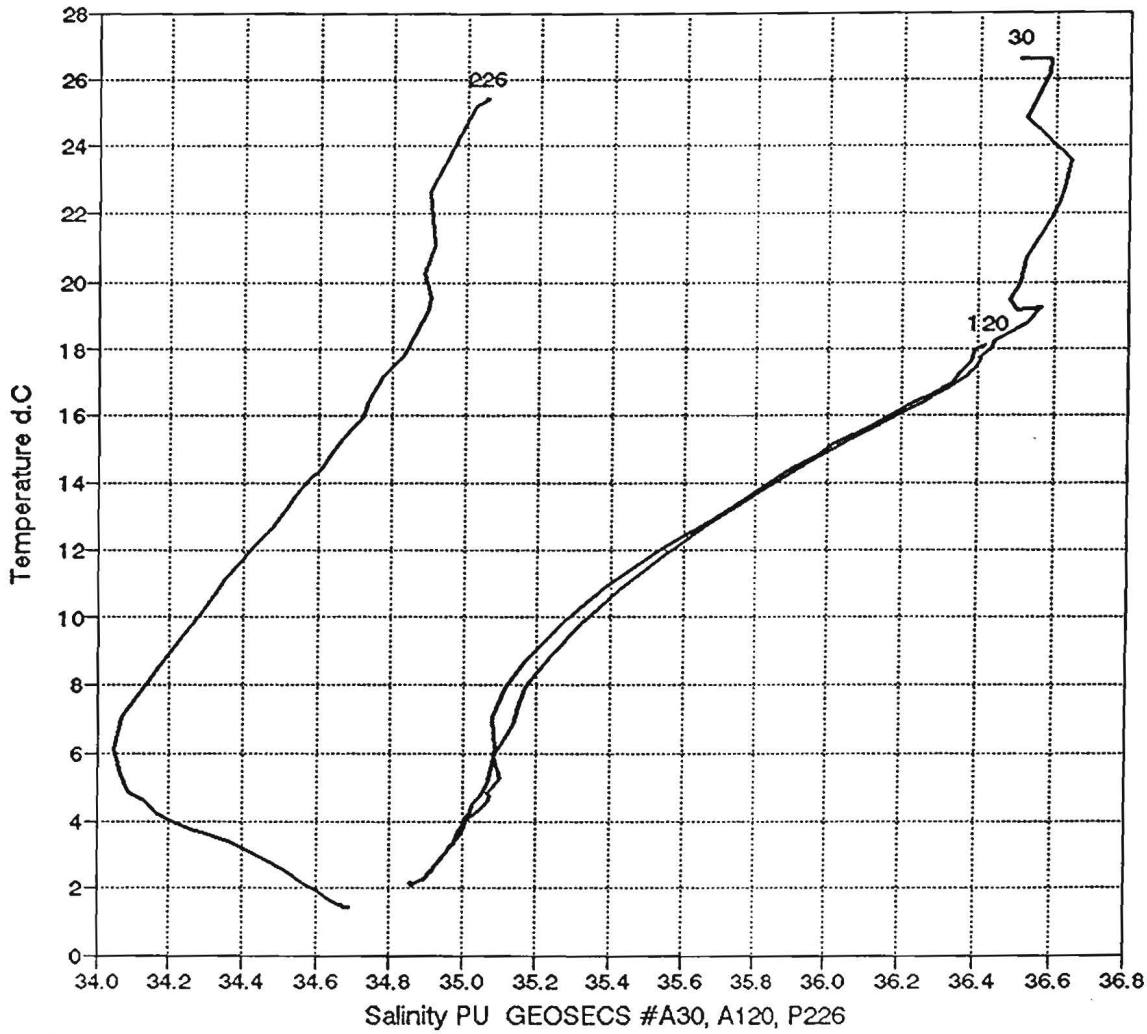

Baumgartner and Reichel (1975) have tabulated the average annual discharges of the 16 largest rivers of Earth. The total discharge amounts to 15,000 km^3 per year. Of these, nine discharge into the Atlantic Ocean and its mediterranean seas, with a total flux of 11,225 km^3 per year, 75 percent of the global annual discharge.

Thus, one has an apparent paradox, the relatively small Atlantic whose waters are diluted by 75 percent of the discharge of the largest rivers of the World has the highest salinity. In contrast, the largest ocean, the Pacific, only receives the discharge of four of the largest rivers with a total discharge of 2,315 km^3, only 15 percent of the total.

Major rivers, however, have a large seasonal variation in their rate of discharge and the atmosphere has only a limited capacity for storing moisture. Peixoto and Oort (1992) have tabulated the annual water budgets in units of E+12 m^3: the atmosphere contains 13 units, compared to a total annual rate of evaporation from the ocean and land surface of 423 units. Of this total, 37 units are discharged annually from the land to the World Ocean.

The paradox arises because one thinks of the fresh water discharge of rivers as diluting the coastal waters. Rather, we should think of the major river basins as reservoirs for the **seasonal** storage for water evaporated from the World Ocean. Large floods, such as the 1993 flooding in Central United States result from the temporary storage of moisture evaporated from the ocean, in this case from the Gulf of Mexico.

Large river basins take water evaporated from the ocean and transported by the wind, store it and then discharge it at their mouth, where it dilutes the coastal waters. The process results is a downward flux of salt in the area of net evaporation and an upward flux of salt in the coastal area of discharge. Whereas the water budget is balanced near the sea surface, the salt budget interacts with the deeper circulation of the ocean.

Let us consider the case of the largest river, the Amazon. The relevant average seasonal variations are shown in **Fig. I-6.4.** Using average runoff data for the period 1968 to 1987 for the total Amazon basin (data from Brazilian Agency DNAEE as published in Nittrouer et al. 1991), one obtains an average monthly discharge, ranging from a maximum of 631 km^3/month in May to a minimum of 281 km^3/month in November. The climatic variations in monthly rainfall amounts in mm/month for three stations in the basin are also shown. They are:

Manaus, M, 3° 6' S, 60° 1' W,
Santarem/Taperinha S, 2° 25' S, 54° 24' W,
Turiacu T, 1° 43' S, 45° 24' W.

Note that the discharge peaks in May after the peak rainfall in April and reaches its minimum value in November following the minimum amount of rainfall in September - October. To infer changes in the ocean, we need to know the change in the mass of water stored in the River basin. Per month, the change in storage is equal to the net addition of precipitation to the basin minus the amount of water discharged by the river at the mouth.

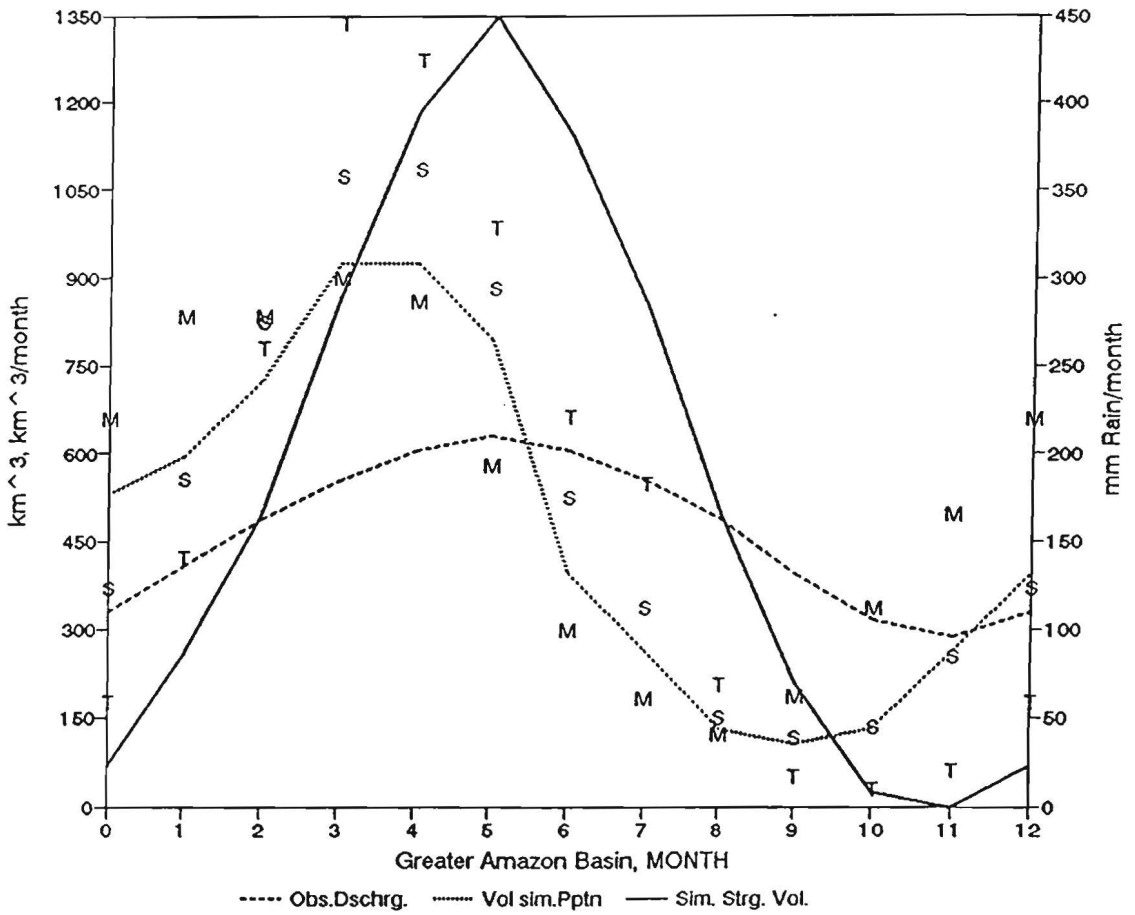

Fig. I-6.4 Annual average cycle of rainfall in mm/month and discharge of the combined Amazon, Tapajos and Xingu River basins (dashed line). The climatic monthly rainfall is for Manaus (M), Santarem/Taperinnha (S) and Turiacu (T). The dotted curve is the simulated net input of rain to the river basin in cubic kilometers/month (dotted curve) and the simulated seasonal cycle of storage of water in the river basin (heavy line) in cubic kilometers.

The amount of water stored in the Amazon basin increases by the difference between the net monthly rainfall and the monthly discharge. The constraint for steady state is that the average annual net rainfall must equal the average annual discharge of 5,655 km^3. The progression of increased discharge does not move downstream with the water, but rather as a shallow water wave, whose speed of advance increases with the square root of the depth of the river. In a deep river like the Amazon, one would therefore expect that the month of maximum/minimum discharge is also the month of maximum/minimum storage.

In the absence of data on the actual seasonal variation of storage in the Amazon basin, I have simulated a **possible** storage volume curve that meets the above constraints. The results are shown in **Fig. I-6.4.** The relative storage of water in the Amazon Basin varies between 1,350 km^3 in May and 0 in November. The area of the North Atlantic between the equator and 30° N is 23 E+6 km^2. Seasonally evaporating 1350 km^3 of seawater from this area is equivalent to evaporating 6 cm of water, thus adding 2,2 gm/m² of sea salt to the water column. If distributed over the upper meter of the water column, this process would raise the salinity by 2 PU during the annual storage cycle.

The seasonal storage of water in the Amazon basin is related to the winds over the Atlantic. From December through April strong winds blow from a north easterly direction onto the Amazon River basin from the Atlantic. The winds weaken in May and June and shift their direction in to blow parallel to the shoreline between July and September from the south east, reducing the rainfall over the Amazon basin.

Thus we have two mechanisms for generating a downward flux of sea salt from the sea surface. Large river basins increase the surface salinity of the ocean by the seasonal storage of fresh water evaporated from the ocean. Partially enclosed seas with net water loss such as the Mediterranean Sea increase the salinity and density of surface ocean water and inject it into the deep ocean across their sills.

Next I investigate the subtropical gyre of North Atlantic, using the abundant oceanographic data from Station "S" near Bermuda.

I-7 STATION "S", SE off BERMUDA

Among the best documented hydrographic stations is Station "S" (WHOI, 1988), South East off Bermuda at 32° 10'N, 64° 30'W, with a water depth of 1750 fathoms. The station is upstream (South East) of the island of Bermuda and water is advected from near the center of the North Atlantic Subtropical Gyre, the section of the gyre having the highest surface salinities in winter (20-30° N, 25-55° W) (Levitus 1982, microfiche F-08 frame 70). The bottle cast observations obtained with R/V Panulirus are listed as cruise #3456 on CD-ROM NODC-02 with a total of 512 stations, covering the period from June 1954 to December 1982.

The annual cycle of surface water temperature at Station "S" is shown in **Fig. I-7.1** as a function of the Day number (Jan.1 = 0). The two digit label for each point is the year of the observation. Also shown is a sine curve with a period of one year whose angle is zero on Day# 155 at a temperature of 23.25° Celsius with an amplitude of ±4.25° C. The sine curve was fitted to the mid point of the steep annual rise in temperature. Note that the observed temperature cycle differs from a sine wave in that the temperature rise in spring is much steeper than the decline in the fall. Also, the duration of the temperature minimum exceeds the period of maximum temperatures.

This asymmetry is due to vertical convection. As the sea surface is heated, the water column becomes stratified so that, at first, a relatively shallow warm layer forms. With surface cooling in the fall, vertical convection deepens gradually, thus slowing down the rate of surface cooling.

The surface salinity as a function of the Day number, **Fig. I-7.2** does not show a significant annual cycle. Instead, the variability increases as the surface temperature increases.

The Density deviation at the surface, **Fig. I-7.3** is essentially an inverted version of the temperature diagram. At station "S", the surface temperature is the dominant determinant of density at the sea surface.

To study the seasonally varying layer, I classify the data from Day# 10 to 120 as "winter" data from Day # 195 to 290 as "summer Data. I then select data close to the following depths 1, 10, 25, 50, 100, 150, 200, 250, 300, 350 and 400 meters, where there are many observations. For each depth I determine the mean value and the standard deviation for the "summer" and "winter" data. I then plot the mean values and the means +/- one standard deviation as a function of the square root of the depth for the temperature Fig. II-2.4, and the salinity Fig. I-7.5.

Fig. I-7.1 Observed Temperature in ° Celsius at Station "S" off Bermuda at 0 or 1 meters depth by day number, label is year. The curve is a sine wave with an amplitude of 4.25 degrees with its origin on day # 155.

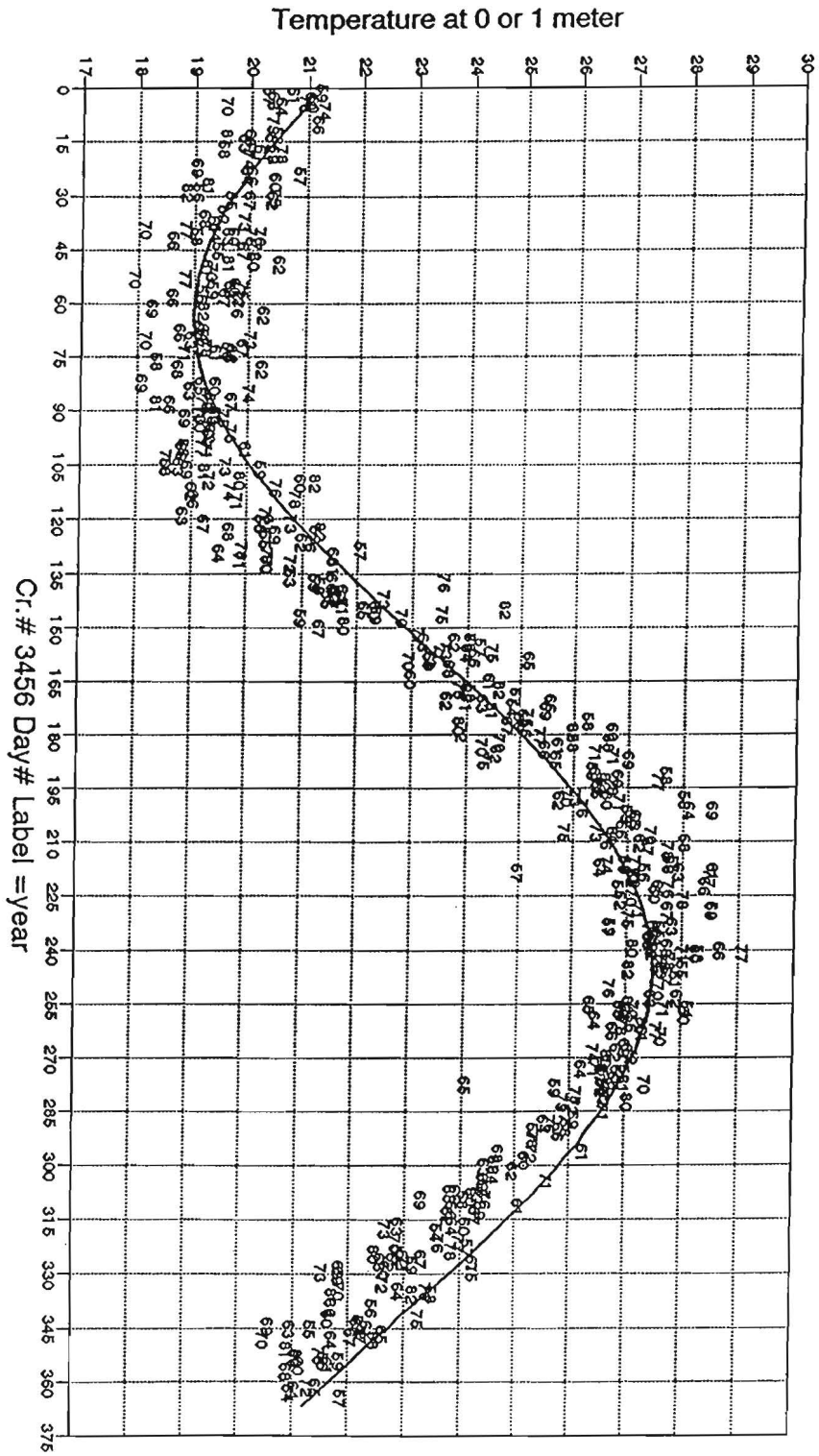

Fig. I-7.2 Observed Salinity in PU at Station "S" off Bermuda at 0 or 1 meters depth by day number, label is year.

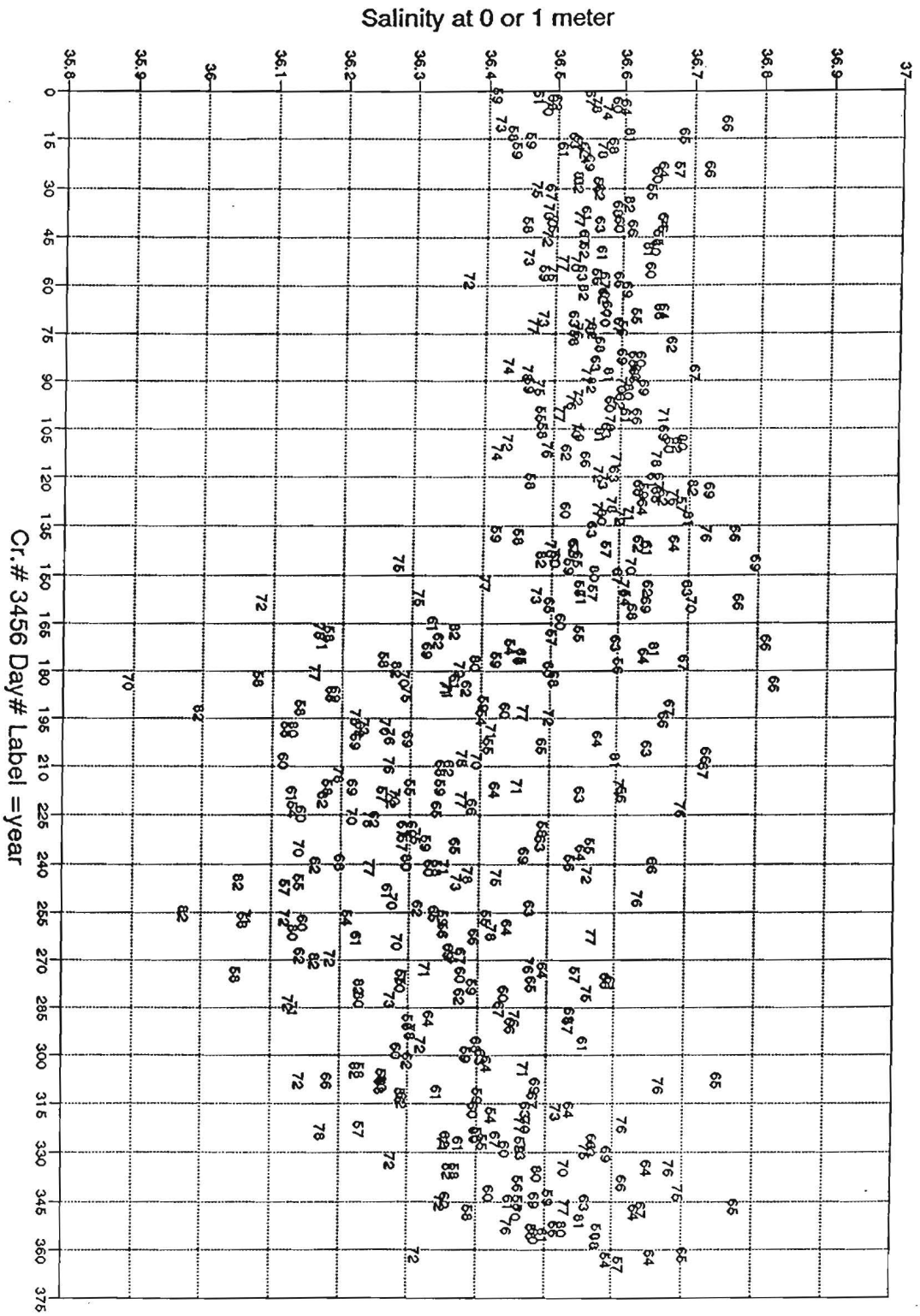

Fig. I-7.3 Observed Density Deviation in kg/m^3 at Station "S" off Bermuda at 0 or 1 meters depth by day number,label is year.

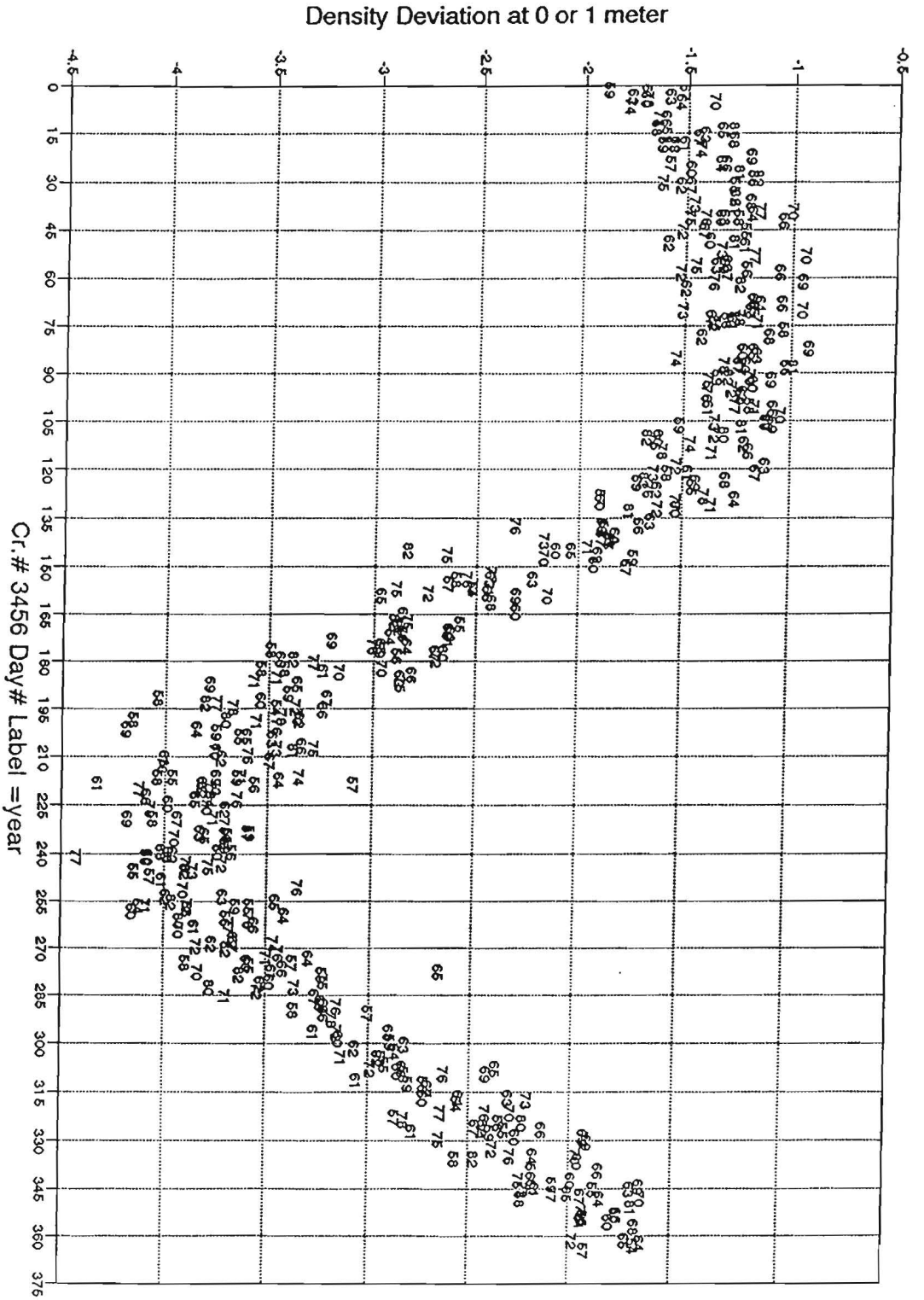

The temperature data **Fig. I-7.4** show that the seasonal cycle penetrates to about 150 meters with a summer mixed layer with a depth ranging from 10 to 25 meters. In "summer", the mean temperature declines sharply from 27° at 10 meters to 20° near 90 meters. The seasonal variation becomes insignificant below 150 meters. The standard deviation of the temperature is 0.7° at 1 meter, increases to 1.4° at 50 meters and declines to 0.4 °C below 200 meters. In "winter" the mean temperature difference between the sea surface and 200 meters is less than 1° and the standard deviation is about 0.6 °C. AT 400 meters, the average temperature is still above 17 °C.

In contrast, the standard deviation of the near surface salinity **Fig. I-7.5** in summer is twice that in winter. Its average value is reduced from a winter value of 36.55 to 36.3 PU.

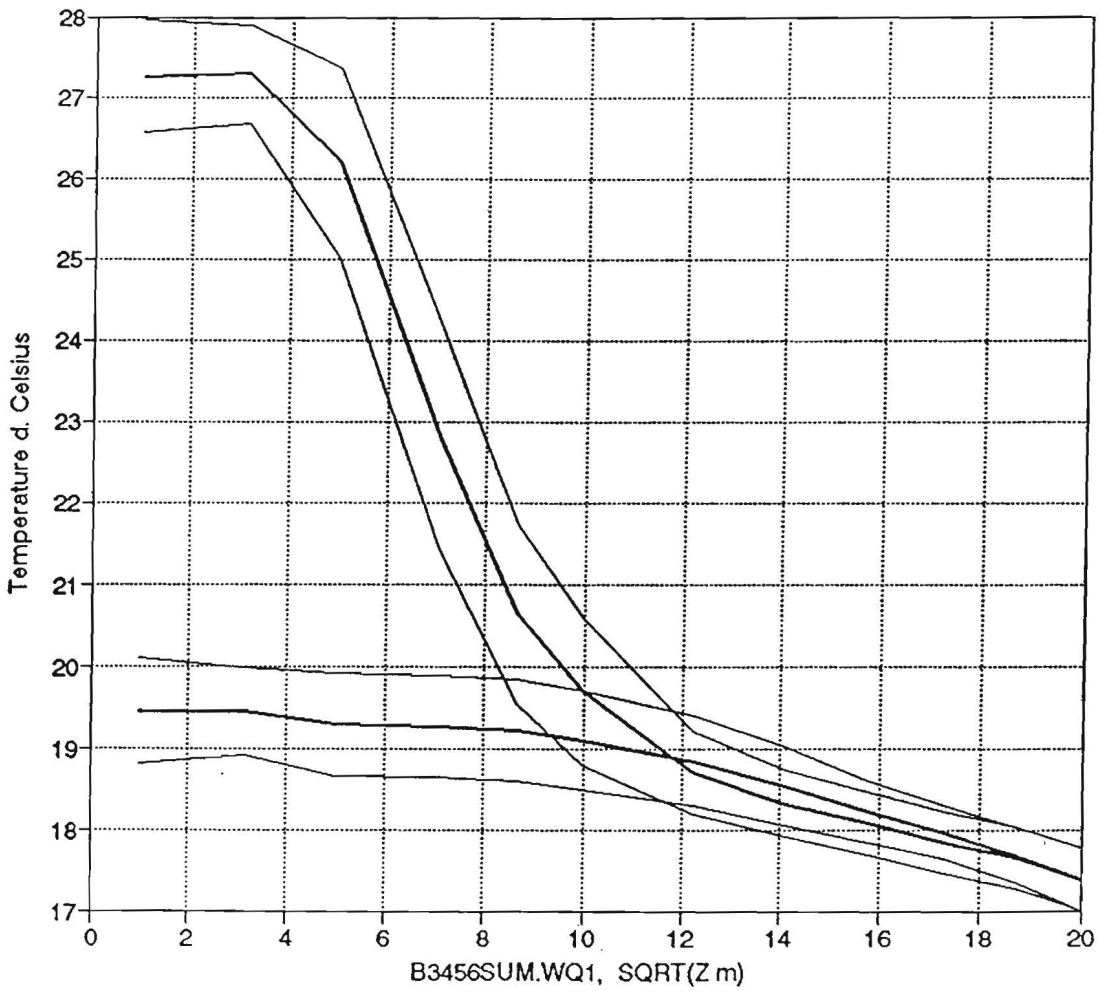

Fig. I-7.4 Average Temperature +/- one standard deviation at Station "S" off Bermuda during "summer" and "winter".

Fig. I-7.5 Average Salinity +/- one standard deviation at Station "S" off Bermuda during "summer" and "winter".

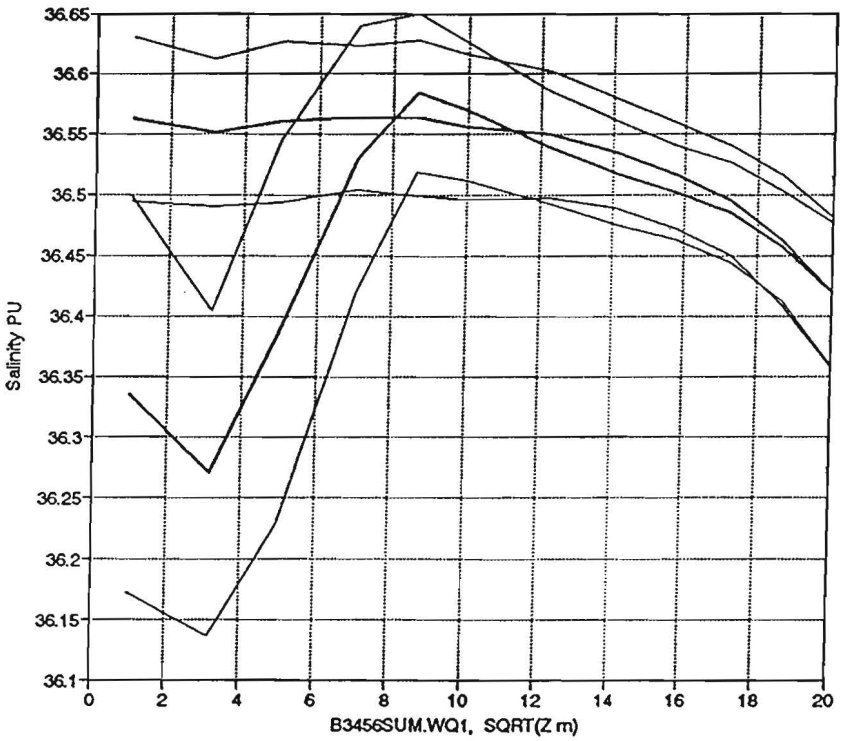

The seasonal cycle does not penetrate below 150 meters. To study the properties of the rest of the water column, I group the data from 150 to 2,600 meters into depth classes of small (at most ± 20 meters) vertical extent and calculate their average properties and standard deviations. The data cover the range in square root of Z(m) from 12 to 52.

Fig. I-7.6 shows the variation of the average temperature and salinity ± one standard deviation. The two curves are similar, however; whereas the salinity curve has a sharp change in slope near SQRT(Z) = 30, the change in slope of the temperature curve is more gradual and occurs at greater depth (SQRT(Z) between 31 and 37)

The variation of density with depth is shown in **Fig. I-7.7.** The gradual change in the density deviation as its value approaches 0.2 kg/m³ indicates that the density in that region is dominated by the temperature.

Fig. I-7.6 Temperature and salinity as a function of the square root of the depth in meters at Station "S". The thin lines to either side indicate the average ± one standard deviation.

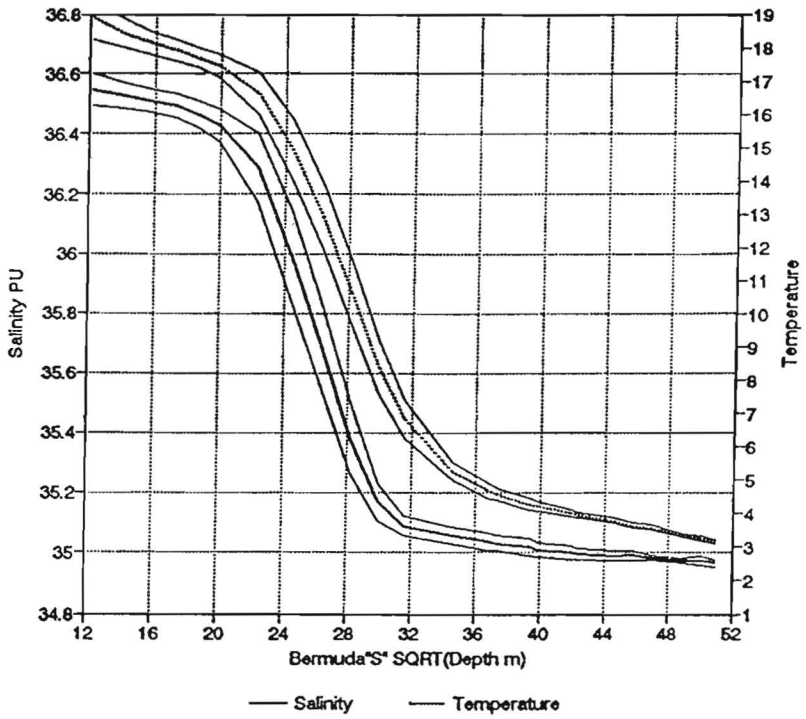

Fig. I-7.7 Density Deviation in kg/m³ as a function of the square root of the depth in meters at Station "S". The thin lines to either side indicate the average ± one standard deviation.

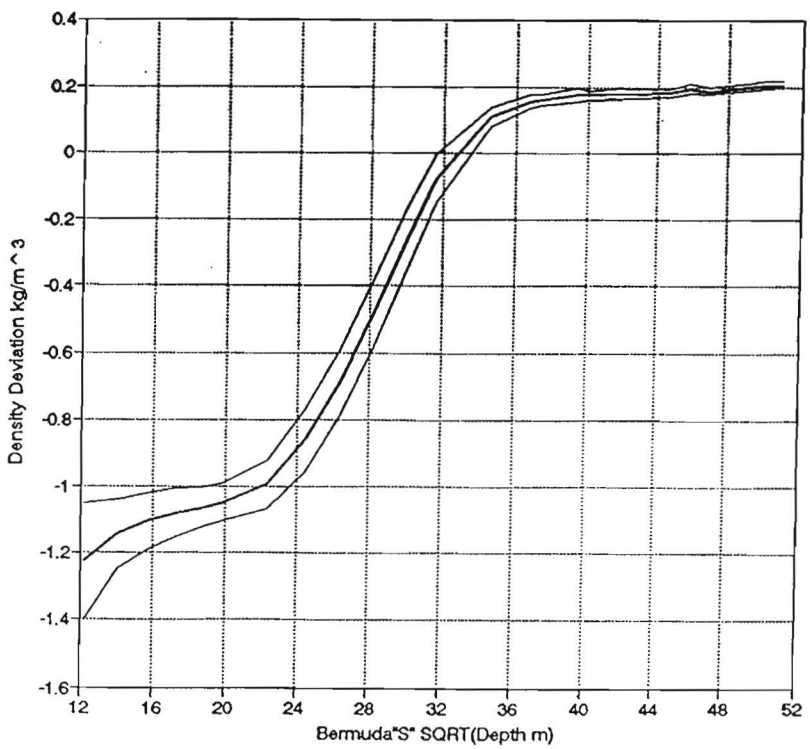

The standard deviation of the density deviation is shown as the heavy line of **Fig. I-7.8.** Note the rapid decrease in the standard deviation to a depth of 400 meters. Then it in-creases to a maximum near 800 meters and then decreases with depth.

To study the extent to which fluctuations in temperature and salinity at a given depth offset each other to maintain a constant density, I proceed as follows. First I determine the standard deviations of the density within a given narrow depth range. Next I assign a random number between zero and one to each observation. I then sort the salinity column to bring the column of random numbers into ascending (or descending) order. After thus randomizing the salinity - temperature association within the limited depth range, I recompute the density deviation for each scrambled temperature - salinity pair.

For large numbers of observations at a particular depth, this will not alter the average density, however; it will increase the standard deviation. The increase in the standard deviation depends on the extent to which the waters had previously been sorted by density. In the absence of sorting, the standard deviation of the density remains the same. If there had been extensive sorting, the randomization of the temperature - salinity pairs will greatly increase the standard deviation.

The dotted line in Fig. I-7.8 indicates the ratio of the standard deviation of the density after randomization to its observed value. At 144 meters, the ratio is close to unity indicating little sorting. It rises to 2.5 times the original value at 600 meters and then declines to 1.3 at 1000 meters.

The primary peak of the standard deviation ratio corresponds to the center of the steep halocline shown in Fig. II-2.6. At either end, the water characteristics maintain their variability by advection. In the halocline, vertical density sorting significantly increases the standard deviation of the density after randomization. The oxygen minimum for station "S" tends to be between 800 and 900 meters, in the lower portion of the standard deviation ratio peak.

A secondary peak in the standard deviation ratio occurs near 1500 meters with a minimum near 2100 meters depth.

Fig. I-7.8 The standard deviation of the observed density as a function of depth and the ratio of its value after/before randomizing temperature - salinity pair's values.

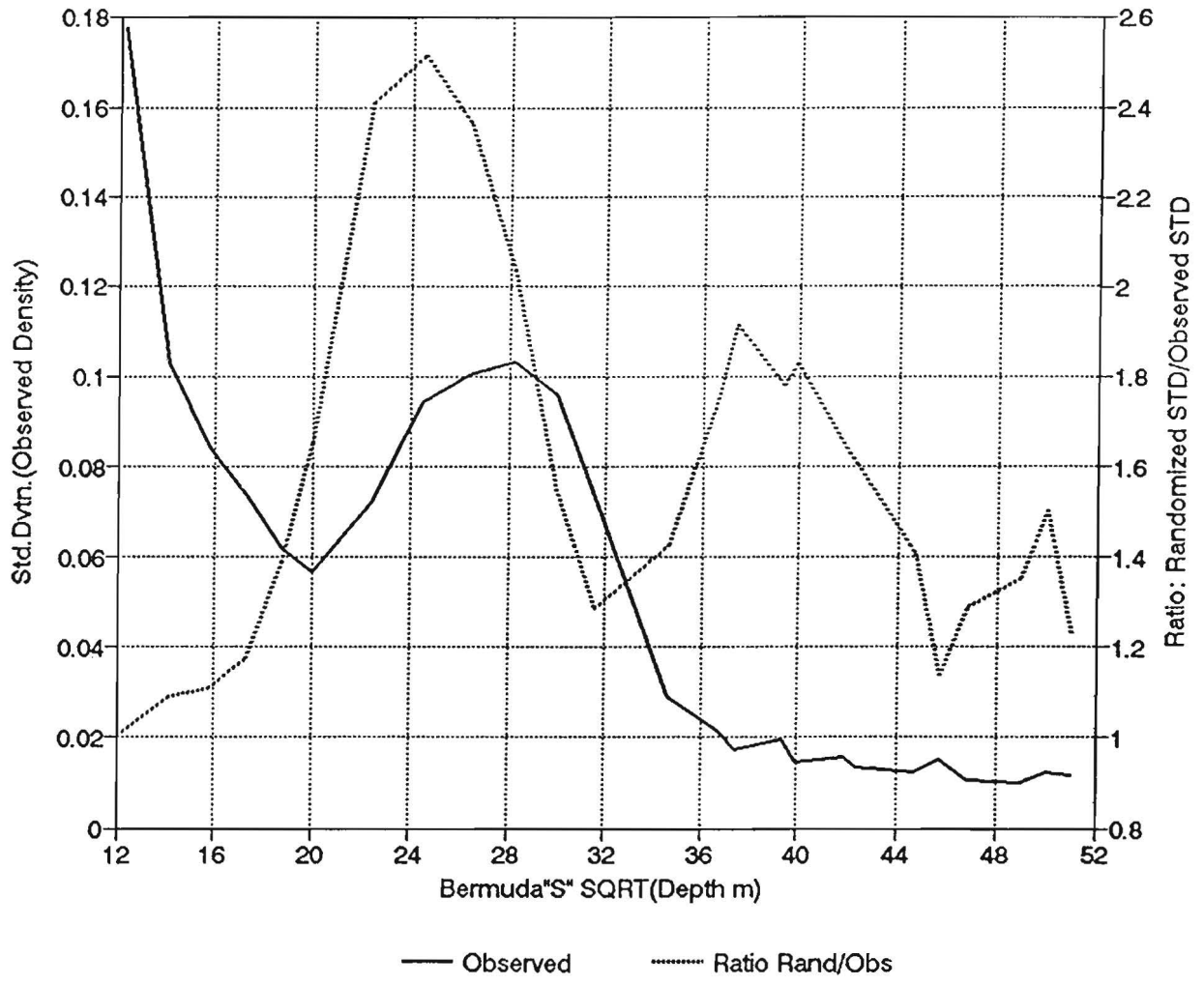

REFERENCES

(Includes references used in suplements to this publication)

CD-ROM from the National Oceanograpic Data Center

CD-ROM NODC-02, Global Ocean Temperature and Salinity Profiles, Vol 1, Atlantic, Indian and Polar Oceans 1981

CD-ROM NODC-03, Global Ocean Temperature and Salinity Profiles, Vol 2, Pacific Ocean, 1981

CD-ROM NODC-20 Oceanographiv Station Profile Time Series

Atlases, Expedition Reports, Data Compilations

E. R. Anderson,Single depth charts of the World Ocean by U.S. Navy Electronics Laboratory , San Diego Cal 1964

H.L. Crutcher and O.M. Davis, 1969, Marine Climatic Atlas of The World, Vol.VII The World, US Navy NAVAIR 50-1C-54

North Atlantic Ocean Atlas of potential temperature and salinity in the Deep Water including temperature, salinity and oxygen profiles from the Erica Dan Cruise of 1962; L.V. Worthington and W.R.Wright, Woods Hole Oceanographic Institution, 1970.

Atlantic Ocean Atlas, Temperature and Salinity Profiles and Data from the International Geophysical Year of 1957-58. F. C. Fuglister, Woods Hole Oceanographic Institution, 1960.

GEOSECS Atlantic Expedition Vol 1, Arnold Bainbridge, Hydrographic Data IDOE, NSF Washington DC August 1981

GEOSECS Atlantic Expedition Vol. 2 Arnold Bainbridge, Sections and Profiles, IDOE, NSF Washington DC

GEOSECS Pacific Expedition Vol 3, Wallace. S. Broecker, Derek W.Spencer and Harmon Craig Hydrographic Data IDOE, NSF Washington DC Oct. 1982

GEOSECS Pacific Expedition Vol. 4 Sections and Profiles, Harmon Craig, Wallace S. Broecker, and Derek Spencer IDOE, NSF Washington DC Oct. 1981

GEOSECS Indian Ocean Expedition Vol 5, Ray F. Weiss, Wallace S. Broecker, Harmon Craig, Derek Spencer Hydrographic Data 1977-1978, NSF Washington DC June 83

GEOSECS Indian Ocean Expedition Vol 6, Sections and Profiles Derek Spencer, Wallace S Broecker, Harmon Craig, Ray F. Weiss, IDOE, NSF Washington DC, Oct 1982

GEOSECS Atlantic, Pacific and Indian Ocean Expedition, Vol. 7 Shorebased Data and Graphics, H. Gote Ostlund, Harmon Craig, Wallace S. Broecker and Derek Spencer, IDOE, NSF Washington DC May 1987

Tansient Tracers in the Ocean, Shipboard Physical and Chemical Data Report, North Atlantic Study, 714 pp. +Appendix; Scripps Institution of Oceanography, UC San Diego 1981

Tansient Tracers in the Ocean, Tropical Atlantic Study,300 pp.;Shipboard Physical and Chemical Data Report, Scripps Institution of Oceanography, UC San Diego 1983

Gordon Arnold L. and Eugene J. Molinelli 1986; Southen Ocean Atlas; 233 plates; Amerind Publishing Co, New Dehli.

Levitus, Sidney; 1982; Climatic Atlas of the World Ocean; NOAA Prof. Paper 13, U.S. Dept. of Commerce, Washington D.C.ME

Station "S" off Bermuda, Physical Measurements, 1954-84; W. G. Metcalf; H. Stommel, W. R. Wright, R. Sherriff-Dow, G. Knapp, R. Stanley, L. Barbour and J. Luyten; Woods Hole Oceanographic Institution and Bermuda Biological Station for Research)

U.S. Navy Hydrographic Office Pub. No 225, 2nd Ed. 1944, World Atlas of Sea Surface Temperatures, Washington DC.

World Weather Records, 1951-60; 1966, vols.1-6. U.S. Department of Commerce, ESSA, Environmental Data Service, U.S.Govt. Printing Office.

Wyrtki, Klaus, 1961, NAGA Report Volume 2, Scientific Results of the South China Sea and the Gulf of Thailand, 1959-61. Physical Oceanography of the Southeast Asian Waters, U. of California, Scripps Institution of Oceanograpy, La Jolla CA.

Wyrtki, Klaus, 1971; Oceanographic Atlas of the International Indian Ocean Expedition; U.S. Govt Printing Office LCCN:73-654319.

Books

Baumgartner, Albert and E. Reichel 1975; The World Water Balance. 180 p. Elsevier, Amsterdam.

L. K. Coachman, K. Aagaard and R. B. Tripp; 1975; Bering Strait, The Regional Physical Oceanography; University of Washington Press, Seattle; 172 pp.

Herman, Yvonne; 1989, Editor; The Arctic Seas, Climatology, Oceanography, Geology and Biology, Van Nostrand Reinhold, New York, 888 pp.

Hopkins T. S. 1988; The GIN Sea, A Revierw of Physical Oceanography and Literature from 1972; SACLANT Report ser # SR-124.

Hurdle,Burton G. Ed.; 1986, The Nordic Seas, Springer Verlag, New York, 777 pp.

Sverdrup, H. U., Johson, M. W. and R. H. Fleming; The Oceans, Their Physics, Chemistry, and General Biology, 1942, Prentice Hall Inc. Englewood Cliffs, N. J.

Schwerdtfeger, W. 1984; Weather and Climate of the Antarctic; 261pp. Elsevier; Amsterdam.

Talley, L. D. and D. Roemmich, 1991; Joseph L. Reid, A Tribute in Recognition of 40 years of Contributions to Oceanography. Deep Sea Research Volume 38, Supplement Issue No. 1A. Pergamon Press, Oxford,

Warren, Bruce A.and Carl Wunsch Ed; 1981; Evolution of Physical Oceanography; MIT Press, Cambridge Mass.

Journal Articles

Aagaard,K. and J. H. Swift and E. C. Carmack, 1985; The Thermohaline Circulation in the Arctic Mediterranean Seas, JGR v.90, pp. 4833-4846.

Anderson L.G., D. W. Dryssen, E. P. Jones and M. G. Lowings; 1983; Inputs and outputs of fresh water, alkalinity, and silica in the Arctic Ocean; Deep Sea Research, v. 30 pp 87-94.

Bryden, H.L. 1973, (Adiabatic Lapse Rate of Seawater) Deep Sea Research, v20 pp. 401-408

Clarke R. Allyn and J. C. Gascard 1983; The Formation of Labrador Sea Water Part I. Large Scale Processes. J. Phys. Oceanog. v. 13, pp.1764-1778.

Clarke R. Allyn and A. R. Coote, 1988; The Formation of Labrador Sea Water Part III: The evolution of Oxygen and Nutrient Concentrations; J.Phys Ocean v.18 pp. 469-480.

Coachman, L. K. and K Aagard, 1988; Transport through Bering Strait: Annual and Interannual Variability, JGR 93 p 15535-15539.

Cosimo J. C. and A.L. Gordon; 1987; Recurring Polynyas over the Cosmonaut Sea and the Maud Rise; JGR 92, pg. 2819-2833.

Deffeyes, K. S., F. J. Lucia and P. K. Weyl, 1965, Dolomitization and limestone diagenises. SEPM Spec. Publ. Nr 13, Lloyd Pray and R. C. Murray Eds. pp.71-88.

Fofonoff, N. P., 1985;Physical Properties of Seawater: A New Salinity Scale and Equation of Stae for Seawater; J. Geophys. Res, v.90 pg3332-3342.

Gascard, J. C. and R. A. Clarke 1983; The Formation of Labrador Sea Water Part II, Mesoscale and smaller scale processes. J. Phys. Oceanogr. v13, 1779-1797.

MEDOC Group, 1970: Observations of formation of deep water in the Mediterranean Sea 1969; Nature, v 227, 1037-1040.

Menard, H. W. and Smith, S. M. Hypsometry of Ocean Basin Provinces, 1966, JGR v.71,pp 4305-4325.

Montgomery, R. B.; 1958; Water Characteristics of Atlantic Ocean and of world Ocean; Deep Sea Research v.5 pp. 134-148.

Olson, Boyd E. 1968; On the Abyssal Temperatures of the World Ocean 151pp. Ph.D Thesis, Oregon State University.

Nittrouer, C. A., DeMaster D. J., Figueirda, A. G. and Rine, J. M. AMASEDS: An Interdisciplinary Investigation of a Complex Coastal Environment, Oceanography Arpril 1991, pg 3-??.

Richardson Philip L. and Schmitz, W. J. Jr. Deep Cross Equatorial Flow in the Atlantic Measured with SOFAR Floats, J. Geophys. Res. v. 98 pp.8371..8387, 1993.

Schmitt, Raymond W.et. al. 1989;Evaporation Minus Precipitation and Density Fluxes in the North Atlantic; J.Phys. Oceanograpphy v.19 pp.1208 - 1221.

Schmitt, Raymond W. 1981; Form of the Temperature-Salinity Relationship in the Central Water: Evidence for double diffuse mixing; J.of Phys. Oceanography v11; pp. 1015-1026.

Van Riel, P. M. 1938; Influence of bottom configuration on properties of Sea Water in abyssal layers. Congrès Intern. de Géographie, Amsterdam 1938, v.2, Travaux Sec.IIb, Océanographie.

Weyl, Peter K. 1961. The Carbonate Saturometer. J. Geology, v.66. pp, 32-44.

1967; The Solution Behaviour of Carbonate Materials in Seawater; in Proceedings of the International Conference on Tropical Oceanography, Nov 1965. University of Miami pp.178-228.

1968; The Role of the Ocean in Climatic Change; A Theory of the Ice Ages; Meteorological Monographs v.8,pp.37-62.

1978 Micropaleontology and the Ocean Surface Climate; 1978; Science v.202 pp.475-481.

Worthington, L. V.; 1981; The Water Masses of the World Ocean, Some results of a fine scale census pp.42-69; in Evolution of Physical Oceanography; Bruce A. Warren and Carl Wunsch Ed; 1981; MIT Press, Cambridge Mass.